Supplementary Information (SI) for Nanoscale.

Supporting Information

Plasmonic Glyco-Nanoparticles for Single-Test Multiplexed Detection and Differentiation of Cancer Cells

A. K. M. Atique Ullah,[a,b] Aniwat Juhong,[b,c] Sherif Ramadan,[a,d] Chia-Wei Yang,[a,b] Zhen Qiu,[b,c,e] Xuefei Huang[a,b,e]*

[a]Department of Chemistry, Michigan State University, East Lansing, MI, 48824 USA

[b]Institute for Quantitative Health Science and Engineering, Michigan State University, East Lansing, MI, 48824 USA

[c]Department of Electrical and Computer Engineering, Michigan State University, East Lansing, MI, 48824 USA

[d]Department of Chemistry, Benha University, Benha 13511, Egypt

[e]Department of Biomedical Engineering, Michigan State University, East Lansing, MI, 48824 USA

Email: huangxu2@msu.edu

Table of contents

Contents

Scheme S1: Schematic representation of synthesis of PlasGlyNPs.

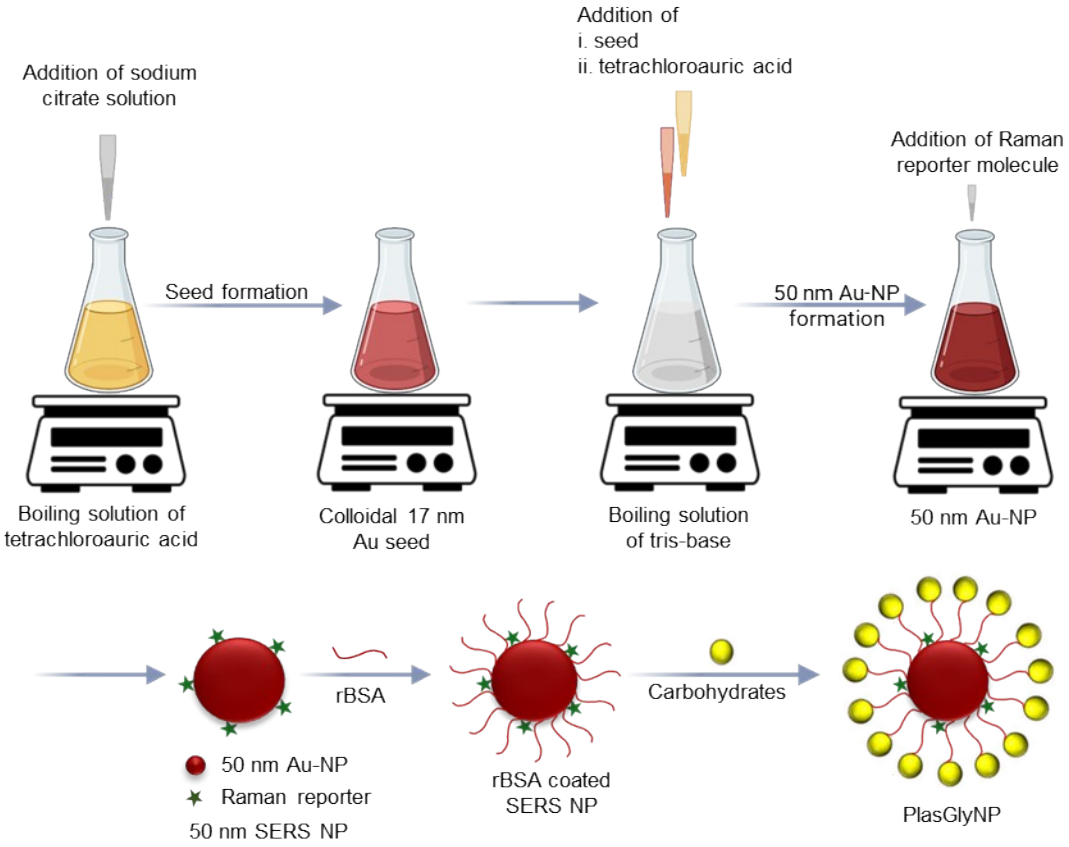

Table S1. Preparative conditions for the synthesis of SERS nanoprobes

Samples	Concentration of rBSA (mg/mL)	LSPR Peak (nm)	Concentration of Fucose Ligand (mg/mL)
DP SERS NP-rBSA0	0	527	
DP SERS NP-rBSA1	0.05	529	
DP SERS NP-rBSA2	0.10	529	
DP SERS NP-rBSA3	0.20	530	
DP SERS NP-rBSA4	0.4	530	

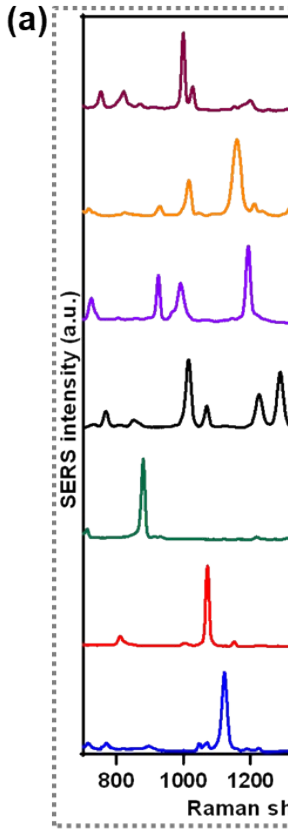

Figure S1. (a) SERS spectra of seven SERS-encoded nanoparticle colloids. From bottom to top: 4-mercaptobenzoic acid (MBA), 4-fluorothiophenol (FTP), 2,3,5,6-tetrafluorobenzenethiol (TFBT), 4,4′-dipyridyl (DP), d8-4,4′-di(pyridyl) (DDP), 4,4′-azobis(pyridine) (ABP), and 2-phenylethanethiol (PET). Representative SERS (1 μM) and Raman (0.1 M) spectra of (b) PET, (c) ABP, and (d) TFBT, showing significant signal enhancement achieved through surface plasmon amplification. The calculated enhancement factors for the seven Raman reporter molecules ranged from 4.4×10^5 to 1.06×10^6.

DP SERS NP-rBSA5	1.0	531	
DP SERS NP-rBSA6	2.0	531	
DP SERS NP-rBSA-Fuc1	1.0	531	0.05
DP SERS NP-rBSA-Fuc2	1.0	531	0.1
DP SERS NP-rBSA-Fuc3	1.0	531	0.2
DP SERS NP-rBSA-Fuc4	1.0	531	0.4
DP SERS NP-rBSA-Fuc5	1.0	531	1
DP SERS NP-rBSA-Fuc5	1.0	531	2

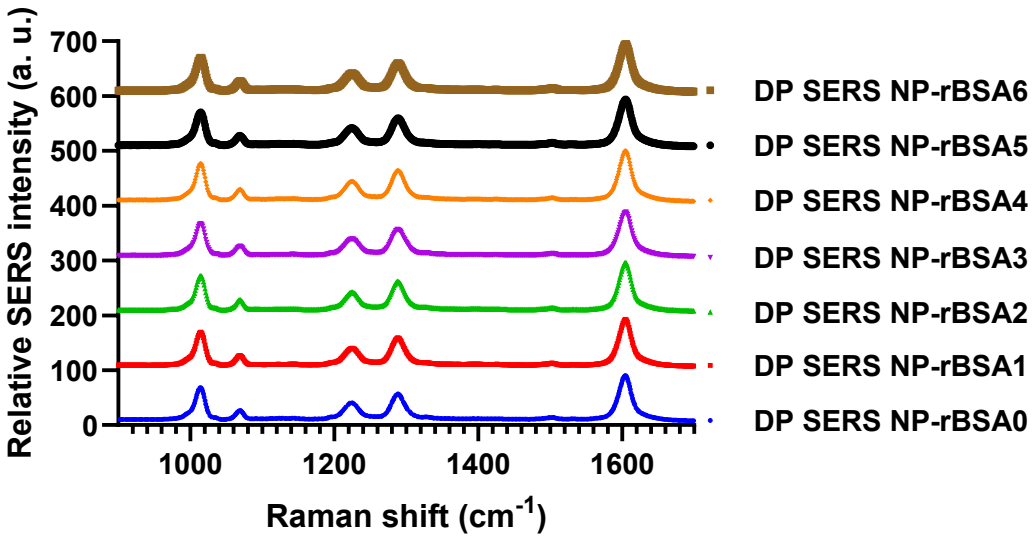

Figure S2. Stacked SERS spectra of 200 pM DP SERS NP–rBSA0–6 plotted in a single axis with vertical offsets to facilitate direct comparison. All spectra were normalized using the intensity of the peak at 1600 cm^{-1} for DP SERS NP–rBSA4 (set as 100%) prior to applying vertical offsets. The nearly identical spectral profiles indicate that rBSA coating does not significantly affect SERS signals.

Scheme S2. Synthesis of Man-ligand

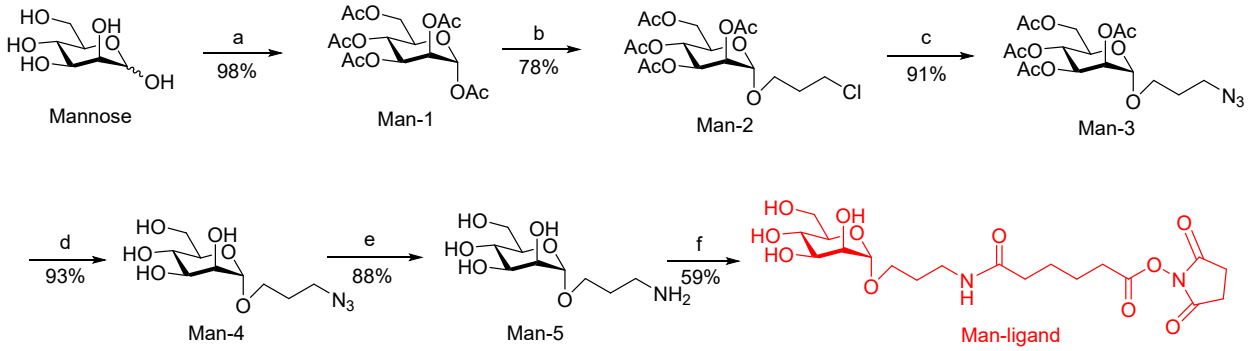

a) Pyririne, acetic anhydride, DMAP, 18 h; b) 3-chloro-1-propanol, $BF_3.Et_2O$, DCM, 18 h; c) NaN_3, DMF, 80 °C, 18 h; d) Na, DCM/MeOH, 3 h; e) H_2, $Pd(OH)_2/C$, 6 h; f) DIPEA, adipic acid di-NHS ester, DMF, 6 h

Azidopropyl 2,3,4,6-tetra-*O*-acetyl-α-D-mannopyranoside (Man-3). Man-3 was prepared as previously described starting from mannose.[1-4] The NMR and HRMS confirmed the structure of Man-3. ^{1}H NMR (500 MHz, $CDCl_3$) δ_H: 5.34 – 5.21 (m, 3H, H-2, H-3, H-4), 4.81 (d, *J* = 1.8 Hz, 1H, H-1), 4.28 (dd, *J* = 12.2, 5.4 Hz, 1H, H-6a), 4.11 (dd, *J* = 12.3, 2.4 Hz, 1H, H-6b), 3.96 (ddd, *J* = 9.6, 5.4, 2.4 Hz, 1H, H-5), 3.81 (ddd, *J* = 9.9, 6.9, 5.5 Hz, 1H, $OCH_aCH_2CH_2N_3$), 3.52 (ddd, *J* = 9.8, 6.4, 5.4 Hz, 1H, $OCH_bCH_2CH_2N_3$), 3.43 (t, *J* = 6.5 Hz, 2H, $OCH_2CH_2CH_2N_3$), 2.16 (s, 3H, OAc), 2.11 (s, 3H, OAc), 2.05 (s, 3H, OAc), 1.99 (s, 3H, OAc), 1.94 – 1.84 (m, 2H, $OCH_2CH_2CH_2N_3$). ^{13}C NMR (125 MHz, $CDCl_3$) δ_C: 170.7, 170.1, 169.9, 169.8, 97.6, 69.5, 69.0, 68.6, 66.1, 64.8, 62.5, 48.1, 28.6, 20.9, 20.74, 20.72, 20.7. HRMS m/z calculated for $C_{17}H_{29}N_4O_{10}$ $[M+NH_4]^+$: 449.1878; found: 449.1868.

Azidopropyl-α-D-mannopyranoside (Man-4). Man-3 (347mg, 0.805 mmol) was deacetylated in a mixture of DCM/MeOH using sodium metal as the reagent. The reaction proceeded for 3 hours at room temperature. Upon completion, the reaction mixture was neutralized using Amberlite 120 (H^+) resin. The resulting solution was filtered, and the solvent was evaporated to yield Man-4 (198 mg) with a 93% yield. ^{1}H NMR (500 MHz, CD_3OD) δ_H: 4.75 (d, *J* = 1.7 Hz, 1H, H-1), 3.88 – 3.77 (m, 3H, H-2, H-6a, $OCH_aCH_2CH_2N_3$), 3.74 – 3.66 (m, 2H, H-3, H-6b), 3.61 (t, *J* = 9.6 Hz, 1H, H-4), 3.54 – 3.46 (m, 2H, H-5, $OCH_bCH_2CH_2N_3$), 3.46 – 3.36 (m, 2H, $OCH_2CH_2CH_2N_3$), 1.90 – 1.82 (m, 2H, $OCH_2CH_2CH_2N_3$). ^{13}C NMR (125 MHz, CD_3OD) δ_C: 100.2, 73.3, 71.2, 70.7, 67.1, 63.9, 61.5, 48.3, 28.5. HRMS m/z calculated for $C_9H_{17}N_3NaO_6$ $[M+Na]^+$: 286.1015; found: 286.1011.

Aminopropyl-α-D-mannopyranoside (Man-5). A mixture of Man-4 (165 mg, 0.627 mmol) and 10% $Pd(OH)_2/C$ (65 mg) in methanol was stirred at room temperature under H_2. After 4 hours, the reaction mixture was filtered through Celite, and the solvent was evaporated to yield Man-5 (131 mg) with an 88% yield. ^{1}H NMR (500 MHz, CD_3OD) δ_H: 4.76 (d, *J* = 1.7 Hz, 1H, H-1), 3.89 – 3.76 (m, 3H, H-2, H-6a, $OCH_aCH_2CH_2NH_2$), 3.76 – 3.64 (m, 2H, H-3, H-6b), 3.60 (t, *J* = 9.7, 1H, H-4), 3.54-3.45 (m, 2H, H-5, $OCH_bCH_2CH_2NH_2$), 2.87 – 2.79 (m, 2H, $OCH_2CH_2CH_2NH_2$), 1.90 – 1.70 (m, 2H, $OCH_2CH_2CH_2NH_2$). ^{13}C NMR (125 MHz, CD_3OH) δ_C: 100.2, 73.4, 71.3, 70.8, 67.2, 64.8, 61.6, 38.2, 30.8. HRMS m/z calculated for $C_9H_{20}NO_6$ $[M+H]^+$: 238.1291; found: 238.1287.

Man-ligand. Man-5 (65 mg, 0.274 mmol) was dissolved in 10 mL of androus DMF. Adipic acid di-NHS ester (478 mg, 0.274 mmol) and DIPEA (35 mg) were added to the solution. The reaction was completed in 8 hours. The product was purified using flash chromatography with a solvent system of 20% methanol in dichloromethane, yielding Man-ligand (75 mg) in 59% yield. ^{1}H NMR

(500 MHz, CD_3OD) δ_H: 4.74 (d, *J* = 1.7 Hz, 1H, H-1), 3.84 (dd, *J* = 11.8, 2.3 Hz, 1H, H-6a), 3.82 – 3.75 (m, 2H, H-2, $OCH_aCH_2CH_2NH$), 3.72 – 3.67 (m, 2H, H-3, H-6b), 3.59 (t, *J* = 9.5 Hz, 1H, H-4), 3.54 – 3.49 (m, 1H, H-5), 3.48-3.42 (m, 1H, $OCH_bCH_2CH_2NH$), 3.31 – 3.20 (m, 2H, $OCH_2CH_2CH_2NH$), 2.84 (s, 4H, $COCH_2CH_2CO$), 2.67 (t, *J* = 6.7 Hz, 2H, $COCH_2CH_2CH_2CH_2CO$), 2.24 (t, *J* = 6.7 Hz, 2H, $COCH_2CH_2CH_2CH_2CO$), 1.82 – 1.76 (m, 2H, $OCH_2CH_2CH_2NH$), 1.76 – 1.70 (m, 4H, $COCH_2CH_2CH_2CH_2CO$). ^{13}C NMR (125 MHz, CD_3OD) δ_C: 174.2, 170.5, 168.7, 100.2, 73.3, 71.2, 70.8, 67.2, 64.6, 61.5, 36.2, 35.1, 29.8, 28.9, 25.1, 24.7, 23.8. HRMS m/z calculated for $C_{19}H_{30}N_2NaO_{11}$ $[M+Na]^+$: 485.1747; found: 485.1745.

Scheme S3. Synthesis of Gal-ligand

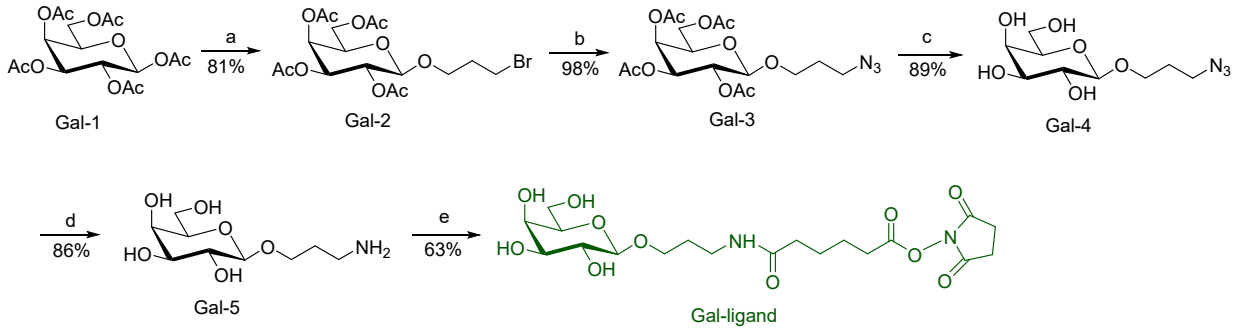

a) 3-bromo-1-propanol, $BF_3.Et_2O$, DCM, 18 h; b) NaN_3, DMF, 80 °C, 18 h; c) Na, DCM/MeOH, 3 h; d) H_2, $Pd(OH)_2/C$, methanol, 6 h; e) DIPEA, adipic acid di-NHS ester, DMF, 6 h

Azidopropyl 2,3,4,6-tetra-*O*-acetyl-β-D-galactopyranoside (Gal-3). Gal-3 was prepared as previously described starting from starting from commercially available pentaacetyl galactose, Gal-1.[5] The NMR and HRMS confirmed the structure of Gal-3. ^1H NMR (500 MHz, $CDCl_3$) δ_H: 5.39 (dd, *J* = 3.5, 1.2 Hz, 1H, H-4), 5.19 (dd, *J* = 10.5, 7.9 Hz, 1H, H-2), 5.01 (dd, *J* = 10.5, 3.4 Hz, 1H, H-3), 4.46 (d, *J* = 7.9 Hz, 1H, H-1), 4.18 (dd, *J* = 11.3, 6.5 Hz, 1H, H-6a), 4.12 (dd, *J* = 11.2, 6.8 Hz, 1H, H-6b), 3.96 (dt, *J* = 9.7, 5.4 Hz, 1H, $OCH_aCH_2CH_2N_3$), 3.91 (td, *J* = 6.7, 1.2 Hz, 1H, H-5), 3.60 (ddd, *J* = 9.7, 8.2, 4.8 Hz, 1H, $OCH_bCH_2CH_2N_3$), 3.45 – 3.31 (m, 2H, $OCH_2CH_2CH_2N_3$), 2.15 (s, 3H, OAc), 2.06 (s, 3H, OAc), 2.05 (s, 3H, OAc), 1.98 (s, 3H, OAc), 1.94 – 1.85 (m, 1H, $OCH_2CH_aCH_2N_3$), 1.85 – 1.75 (m, 1H, $OCH_2CH_bCH_2N_3$). ^{13}C NMR (125 MHz, $CDCl_3$) δ_C: 170.4, 170.3, 170.2, 169.5, 101.3, 77.3, 77.3, 77.1, 76.8, 70.9, 70.7, 68.8, 67.0, 66.5, 61.3, 47.9, 28.9, 20.8, 20.68, 20.67, 20.6. HRMS m/z calculated for $C_{17}H_{29}N_4O_{10}$ $[M+NH_4]^+$: 449.1878; found: 449.1875.

Azidopropyl-β-D-galactopyranoside (Gal-4). Gal-3 (579 mg, 1.343 mmol) was deacetylated in a mixture of DCM/MeOH using sodium metal as the reagent. The reaction proceeded for 3 hours at room temperature. Upon completion, the reaction mixture was neutralized using Amberlite 120 (H^+) resin. The resulting solution was filtered, and the solvent was evaporated to yield Gal-4 (315 mg) with a 89% yield. ^1H NMR (500 MHz, CD_3OD) δ_H: 4.21 (d, *J* = 7.4 Hz, 1H, H-1), 3.97 (dt, *J* = 10.0, 6.0 Hz, 1H, $OCH_aCH_2CH_2N_3$), 3.84 (dd, *J* = 3.3, 1.1 Hz, 1H, H-4), 3.81 – 3.69 (m, 2H, H-6), 3.64 (dt, *J* = 10.1, 6.1 Hz, 1H, $OCH_bCH_2CH_2N_3$), 3.55 – 3.49 (m, 2H, H-2, H-5), 3.49 – 3.41 (m, 3H, H-3, $OCH_2CH_2CH_2N_3$), 1.87 (m, 2H, $OCH_2CH_2CH_2N_3$). ^{13}C NMR (125 MHz, CD_3OD) δ_C:

103.7, 75.2, 73.5, 71.1, 68.8, 66.1, 61.0, 48.0, 28.9. HRMS m/z calculated for $C_9H_{17}N_3NaO_6$ $[M+Na]^+$: 286.1015; found: 286.1001.

Aminopropyl-β-D-galactopyranoside (Gal-5).

A mixture of Gal-4 (183 mg, 0.696 mmol) and 10% $Pd(OH)_2/C$ (91 mg) in methanol was stirred at room temperature under H_2. After 4 hours, the reaction mixture was filtered through Celite, and the solvent was evaporated to yield Gal-5 (142 mg) with an 86% yield. ^1H NMR (500 MHz, CD_3OD) δ_H: 4.28 (d, *J* = 6.8 Hz, 1H, H-1), 4.02 (ddd, *J* = 10.4, 6.9, 4.5 Hz, 1H, $OCH_aCH_2CH_2NH_2$), 3.83 (dd, *J* = 2.9, 1.1 Hz, 1H, $OCH_bCH_2CH_2NH_2$), 3.82 – 3.76 (m, 1H, H-3), 3.76 – 3.72 (m, 2H, H-6), 3.57 – 3.52 (m, 1H, H-5), 3.52 – 3.46 (m, 2H, H-2, H-4), 3.12 (m, 2H, $OCH_2CH_2CH_2NH_2$), 1.97 (m, 2H, $OCH_2CH_2CH_2NH_2$). ^{13}C NMR (126 MHz, CD_3OD) δ_C: 103.6, 75.5, 73.5, 71.0, 68.9, 67.4, 61.1, 37.9, 26.9. HRMS m/z calculated for $C_9H_{20}NO_6$ $[M+H]^+$: 238.1291; found: 238.1286.

Gal-ligand. Gal-5 (93 mg, 0.392 mmol) was dissolved in 10 mL of dry DMF. Adipic acid di-NHS ester (685 mg, 1.961 mmol) and DIPEA (51 mg) were added to the solution. The reaction was completed in 8 hours. The product was purified using flash chromatography with a solvent system of 20% methanol in dichloromethane, yielding Gal-ligand (114 mg) in 63% yield. ^1H NMR (500 MHz, CD_3OD) δ_H: 4.22 (d, *J* = 7.4 Hz, 1H, H-1), 3.94 (dt, *J* = 9.9, 6.0 Hz, 1H, $OCH_aCH_2CH_2NH_2$), 3.83 (d, *J* = 3.2 Hz, 1H, H-5), 3.78 – 3.68 (m, 2H, $OCH_bCH_2CH_2NH_2$, H-3), 3.62 (dd, *J* = 11.1, 5.2 Hz, 1H, H-3), 3.56 – 3.44 (m, 3H, H-2, H-4,), 3.39 – 3.32 (m, 2H, H-6), 2.84 (s, 4H, $COCH_2CH_2CO$), 2.68 (t, *J* = 6.7 Hz, 2H, $COCH_2CH_2CH_2CH_2CO$), 2.24 (t, *J* = 6.7 Hz, 2H, $COCH_2CH_2CH_2CH_2CO$), 1.84 – 1.76 (m, 2H, $OCH_2CH_2CH_2NH$), 1.77 – 1.66 (m, 4H, $COCH_2CH_2CH_2CH_2CO$). ^{13}C NMR (125 MHz, CD_3OD) δ_C: 174.3, 170.5, 168.7, 103.6, 75.3, 73.6, 71.2, 68.9, 66.9, 61.2, 36.2, 35.1, 29.8, 28.9, 25.1, 24.7, 23.8. HRMS m/z calculated for $C_{19}H_{30}N_2NaO_{11}$ $[M+Na]^+$: 485.1747; found: 485.1723.

Scheme S4. Synthesis of Fuc-ligand

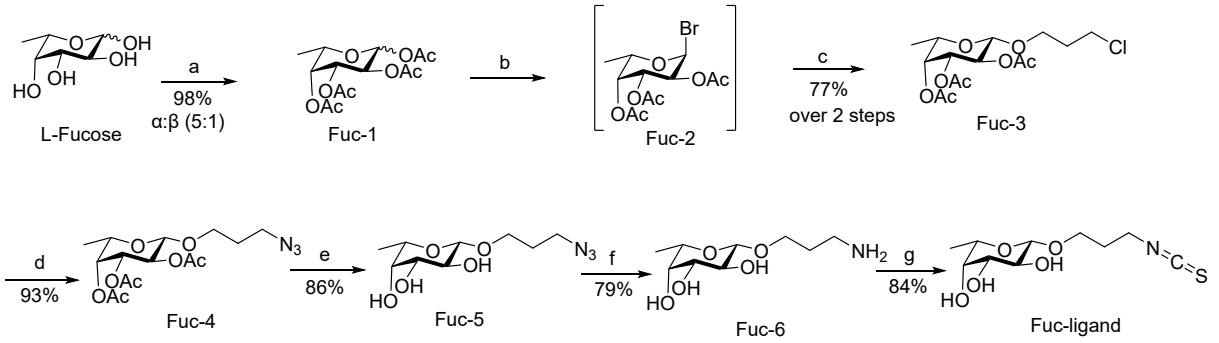

Reagents and conditions: a) pyridine, acetic anhydride, DMAP, 12 h; b) 33 % HBr in acetic acid, DCM, 6 h; c) 3-cholor-1-propanol, 4Å MS, Ag_2CO_3, DCM, 18 h; d) NaN_3, DMF, 80 °C, 18 h; e) Na, MeOH, 4 h; f) $H_2/Pd(OH)_2$-C, MeOH, 4 h; e) thiophosgene, H_2O:$CHCl_3$ (2:3, v/v), 6 h

Azidopropyl-2,3,4-tri-*O*-acetyl-β-L-fucose (Fuc-4). Fuc-4 was prepared as previously described starting from L-Fucose.[6] The NMR and HRMS confirmed the structure of Fuc-4. ^1H NMR (500 MHz, $CDCl_3$) δ_H: 5.23 (dd, *J* = 3.5, 1.1 Hz, 1H, H-4), 5.17 (dd, *J* = 10.5, 7.9 Hz, 1H, H-2), 5.01 (dd, *J* = 10.5, 3.5 Hz, 1H, H-3), 4.43 (d, *J* = 7.9 Hz, 1H, H-1), 3.97 (m, 1H,

OC*H*$_a$HCH$_2$CH$_2$N$_3$), 3.81 (m, 1H, H-5), 3.57 (m, 1H, OCH*H*$_b$CH$_2$CH$_2$N$_3$), 3.41 – 3.32 (m, 2H, OCH$_2$CH$_2$C*H*$_2$N$_3$), 2.17, 2.06, 1.98 (3s, 3 x 3H, CH3CO), 1.95 – 1.85 (m, 1H, OCH$_2$C*H*$_a$CH$_2$N$_3$), 1.84 – 1.73 (m, 1H, OCH$_2$C*H*$_b$CH$_2$N$_3$), 1.22 (d, *J* = 6.4 Hz, 3H, H-6). ^{13}C NMR (125 MHz, $CDCl_3$) δ_C: 170.7, 170.2, 169.6, 101.2, 71.3, 70.2, 69.2, 69.0, 66.3, 48.0, 29.0, 20.8, 20.7, 20.6, 16.0. HRMS m/z calculated for $C_{15}H_{23}N_3NaO_8$ $[M+Na]^+$: 396.1383; found: 396.1370.

Azidopropyl-β-L-fucose (Fuc-5). To a solution of Fuc-4 in methanol (680 mg, 1.822 mmol), sodium metal was added to adjust the pH of the reaction mixture to 10. The reaction was completed within 4 hours at room temperature. The solution was then neutralized using Amberlite 120 (H^+) resin. The reaction mixture was filtered, and the solvent was evaporated. The product was purified by flash chromatography using 10% methanol in dichloromethane, yielding Fuc-5 (387 mg) in 86% yield. ^{1}H NMR (500 MHz, CD_3OD): δ_H: 1.27 (d, *J* = 6.5 Hz, 3H), 1.87 (m, 2H, OCH$_2$C*H*$_2$CH$_2$N$_3$), 3.51–3.42 (m, 4H, H-2, H-4, OCH$_2$CH$_2$C*H*$_2$N$_3$), 3.68–3.59 (m, 3H, H-3, H-5, OC*H*$_a$HCH$_2$CH$_2$N$_3$), 3.92 (m, 1H, OCH*H*$_b$CH$_2$CH$_2$N$_3$), 4.20 (d, *J* = 7.6 Hz, 1H, H-1). ^{13}C NMR (125 MHz, CD_3OD) δ_C: 15.4, 28.9, 48.1, 66.2, 70.5, 70.9, 71.6, 73.7, 103.5. HRMS m/z calculated for $C_9H_{17}N_3NaO_5$ $[M+Na]^+$: 270.1066; found: 270.1067.

Aminopropyl-β-L-fucose (Fuc-6). A mixture of Fuc-5 (230 mg, 0.931 mmol) and 10% $Pd(OH)_2/C$ (95 mg) in methanol was stirred at room temperature under H_2. After 6 hours, the reaction mixture was filtered through Celite, and the solvent was evaporated to yield Fuc-6 (163 mg) with an 79% yield. ^{1}H NMR (500 MHz, D_2O): δ_H: 1.07 (d, *J* = 6.4 Hz, 3H, H-6), 1.92-1.51 (m, 2H, OCH$_2$C*H*$_2$CH$_2$NH$_2$), 2.86 (t, *J* = 7.2 Hz, 2H, OCH$_2$CH$_2$C*H*$_2$NH$_2$), 3.29 (dd, *J* = 10.2, 7.9 Hz, 1H, H-2), 3.46 (dd, *J* = 9.9, 3.5 Hz, 1H, H-3), 3.53–3.64 (m, 3H, H-4, H-5, OC*H*$_a$HCH$_2$CH$_2$NH$_2$), 3.80 (m, 1H, OC*H*$_b$HCH$_2$CH$_2$NH$_2$), 4.20 (d, *J* = 7.9 Hz, 1H, H-1). ^{13}C NMR (125 MHz, D_2O) δ_C: 15.3, 26.4, 45.6, 67.7, 70.4, 70.8, 71.2, 72.8, 102.5. HRMS m/z calculated for $C_9H_{19}NNaO_5$ $[M+H]^+$: 222.1341; found: 222.1340.

Fuc-ligand. Fuc-6 (142 mg, 0.642 mmol) was dissolved in a $NaHCO_3$ solution (10 mg/mL), then chloroform containing thiophosgene (246 µL, 3.21 mmol) was added. The mixture was stirred vigorously at room temperature for 6 hours. After the reaction was complete, the reaction mixture was diluted with water, and the aqueous layer was extracted three times with chloroform to remove excess thiophosgene. The aqueous layer was collected, dried, and purified using G-10 column, yielding the Fuc-ligand (142 mg) with an 84% yield. ^{1}H NMR (500 MHz, D_2O) δ_H: 4.33 (d, *J* = 7.9 Hz, 1H, H-1), 3.93 (dt, *J* = 10.5, 6.1 Hz, 1H, OC*H*$_a$CH$_2$CH$_2$NCS), 3.78 – 3.69 (m, 3H, H-4, H-5, OC*H*$_b$CH$_2$CH$_2$NCS), 3.68 (t, *J* = 6.5 Hz, 2H, OCH$_2$CH$_2$C*H*$_2$NCS), 3.61 (dd, *J* = 10.0, 3.5 Hz, 1H, H-3), 3.44 – 3.36 (m, 1H, H-2), 1.95 (m, 2H, OCH$_2$C*H*$_2$CH$_2$NCS), 1.20 (d, *J* = 6.3 Hz, 3H, H-6). ^{13}C NMR (126 MHz, D_2O) δ_C: 160.5, 102.8, 72.9, 71.4, 71.0, 70.6, 66.9, 41.8, 29.1, 15.6. HRMS m/z calculated for $C_{10}H_{17}NNaO_5S$ $[M+Na]^+$: 286.0725; found: 286.0726.

Scheme S5. Synthesis of GlcNAc-ligand

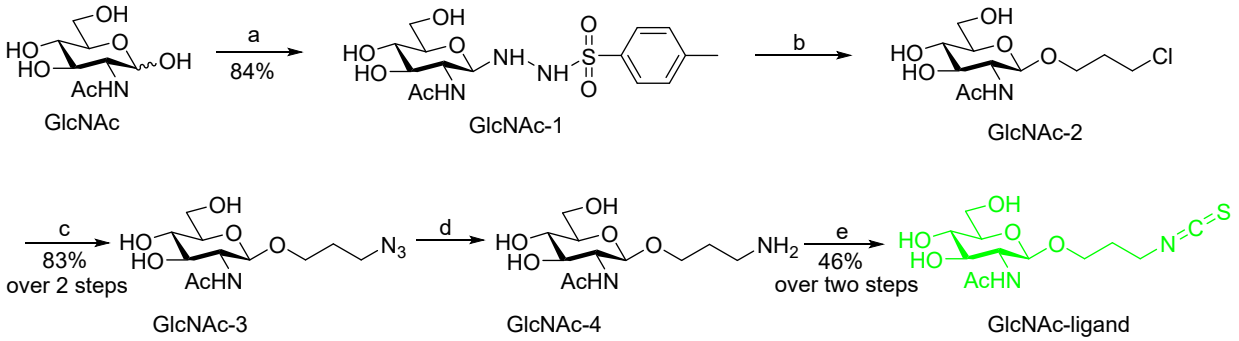

a) NH_2NHTs, acetic acid, DMF, H_2O, 37 °C, 2 days; b) 3-chloro-1-propanol, NBS, DMF, 18 h; c) NaN_3, DMF, 80 °C, 18 h; e) $Pd(OH)_2/C$, methanol, 12 h; f) thiophosgene, H_2O:$CHCl_3$ (2:3, v/v), 6 h.

3-Azidopropyl-β-D-GlcNAc (GlcNAc-3). GlcNAc-3 was prepared as previously described starting from starting from GlcNAc.[7] The NMR and HRMS confirmed the structure of GlcNAc-3. ^{1}H NMR (500 MHz, D_2O) δ_H: 4.34 (d, *J* = 8.5 Hz, 1H, H-1), 3.84 – 3.78 (m, 1H, $OCH_aCH_2CH_2N_3$), 3.76 (dd, *J* = 12.3, 1.8 Hz, 1H, H-6a), 3.58 (dd, *J* = 12.4, 5.6 Hz, 1H, H-6b), 3.55 – 3.47 (m, 2H, H-2, $OCH_bCH_2CH_2N_3$), 3.40 – 3.34 (m, 1H, H-4), 3.31 – 3.25 (m, 2H, H-3, H-5), 3.24-3.18 (m, 2H, $OCH_2CH_2CH_2N_3$), 1.88 (s, 3H, $NHCOCH_3$), 1.72 – 1.62 (m, 2H, $OCH_2CH_2CH_2N_3$). ^{13}C NMR (125 MHz, D_2O) δ_C: 174.4, 101.1, 75.7, 73.6, 69.8, 67.0, 60.6, 55.5, 47.7, 28.0, 22.0. HRMS m/z calculated for $C_{11}H_{20}N_4NaO_6$ $[M+Na]^+$: 327.1281; found: 327.1244.

GlcNAc Ligand. A mixture of GlcNAc-3 (198 mg, 0.651 mmol) and 10% $Pd(OH)_2/C$ (76 mg) in methanol was stirred at room temperature under H_2. After 6 hours, the reaction mixture was filtered through Celite, and the solvent was evaporated to yield GlcNAc-4. The residue was then dissolved in 5 mL $NaHCO_3$ solution (10 mg/mL), followed by the addition of 7.5 mL of chloroform containing thiophosgene (250 µL, 3.25 mmol). The mixture was stirred vigorously at room temperature for 6 hours. After the reaction was complete, the reaction mixture was diluted with water, and the aqueous layer was extracted three times with chloroform to remove excess thiophosgene. The aqueous layer was collected, dried, and purified using a G-10 column, yielding the GlcNAc-ligand (96 mg) in 46% yield over two steps. ^{1}H NMR (500 MHz, D_2O) δ_H: 4.35 (d, *J* = 8.4 Hz, 1H, H-1), 3.91 – 3.84 (m, 1H, m, 1H, $OCH_aCH_2CH_2NCS$), 3.77 (dd, *J* = 12.3, 1.9 Hz, 1H, H-6a), 3.61 – 3.56 (m, 1H, H-6b), 3.56 – 3.50 (m, 2H, H-2, $OCH_bCH_2CH_2NCS$), 3.50 – 3.44 (m, 2H, $OCH_2CH_2CH_2N_3$), 3.41 – 3.36 (m, 1H, H-4), 3.32 – 3.25 (m, 2H, H-3, H-5), 1.91 (s, 3H, $NHCOCH_3$), 1.83 – 1.75 (m, 2H, $OCH_2CH_2CH_2N_3$). ^{13}C NMR (125 MHz, D_2O) δ_C: 174.6, 160.3, 101.4, 75.8, 73.6, 69.9, 66.6, 60.7, 55.6, 41.4, 28.8, 22.3. HRMS m/z calculated for $C_{12}H_{20}N_2NaO_6S$ $[M+Na]^+$: 343.0940; found: 343.0951.

Scheme S6. Synthesis of Sia-ligand

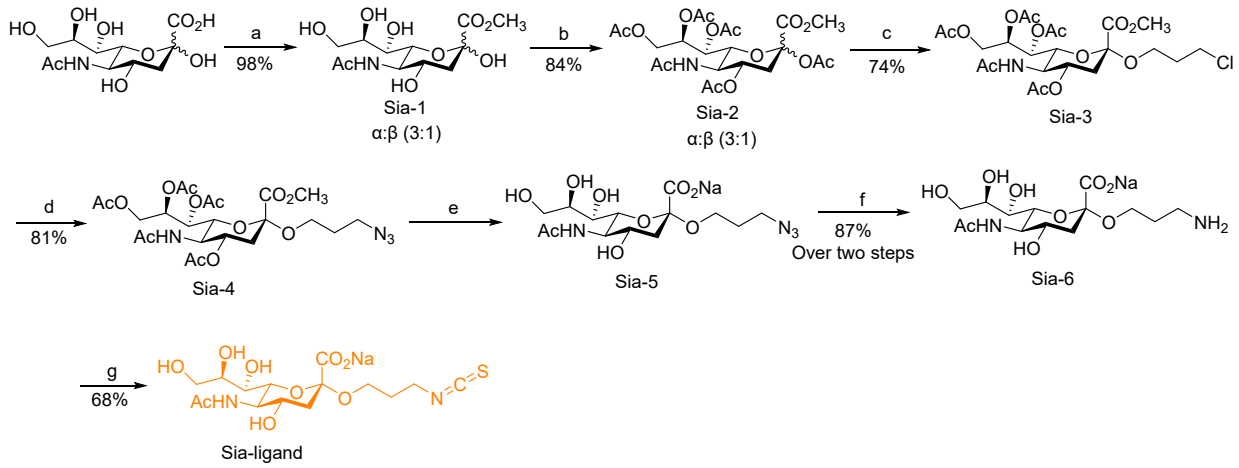

a) Amberlite H-form, MeOH, 24 h; b) Pyririne, acetic anhydride, DMAP, 18 h; c) 3-chloro-1-propanol, $BF_3.Et_2O$, DCM, 18 h; d) NaN_3, DMF, 80 ^oC, 18 h; e) NaOH, DCM, MeOH, 3 h; f) $Pd(OH)_2/C$, 6 h; g) thiophosgene, H_2O, $CHCl_3$ (2:3, v/v)

***O*-Acetyl sialic azide (Sia-4).** Sia-4 was prepared as previously described starting from starting from Sialic acid.[6] The NMR and HRMS confirmed the structure of Sia-4. ^{1}H NMR (500 MHz, $CDCl_3$) for α-anomer, δ_H: 5.41 (dd, *J* = 3.7, 2.3 Hz, 1H, H-7), 5.26 – 5.20 (m, 2H, H-4, H-8), 4.83 (dd, *J* = 12.4, 2.5 Hz, 1H, H-9a), 4.16 – 4.05 (m, 2H, H-5, H-9b), 3.96 (dd, *J* = 10.6, 2.3 Hz, 1H, H-6), 3.82 (s, 3H, CO_2CH_3), 3.65 – 3.57 (m, 1H, $OCH_2CH_2CH_aN_3$), 3.54 – 3.36 (m, 3H, $OCH_2CH_2CH_2N_3$,$OCH_2CH_2CH_bN_3$), 2.46 (dd, *J* = 12.9, 4.9 Hz, 1H, H-3$_{eq}$), 2.16, 2.09, 2.04, 2.03, 1.89 (5s, 5 x 3H, $COCH_3$), 1.92 - 1.88 (m, 1H, H-3$_{ax}$), 1.87 - 1.82 (m, 2H, $OCH_2CH_2CH_2N_3$). ^{13}C NMR (125 MHz, $CDCl_3$) δ_C: 171.0, 170.8, 170.6, 170.25, 170.20, 167.4, 98.6, 72.1, 71.9, 68.7, 68.6, 62.4, 60.6, 52.9, 49.3, 48.1, 37.4, 28.7, 23.2, 21.0, 20.9, 20.83, 20.82. HRMS m/z calculated for $C_{23}H_{35}N_4O_{13}$ $[M+H]^+$: 575.2201; found: 575.2190.

Sialic amine (Sia-6). To a solution of Sia-4 (314 mg, 0.547 mmol) in methanol/dichloromethane, 5 mL sodium hydroxide (218 mg, 5.46 mmol) solution was added. The reaction was completed within 6 hours at room temperature. The solution was then neutralized using Amberlite 120 (H^+) resin. The reaction mixture was filtered and evaporated, yielding Sia-5. A mixture of Sia-5 and 80 mg 10% $Pd(OH)_2/C$ in methanol was stirred at room temperature under H_2. After 6 hours, the reaction mixture was filtered through Celite, and the solvent was evaporated to yield Sia-6 (165 mg) with a 94% yield.^{1}H NMR (500 MHz, D_2O) δ_H: 3.96 – 3.83 (m, 1H, H-4), 3.72 – 3.64 (m, 4H, H-5, H-7, H-8, H-9a), 3.62 – 3.54 (m, 1H, $OCH_aCH_2CH_2NH_2$), 3.53 – 3.45 (m, 1H, H-9b), 3.40 – 3.32 (m, 1H, H-6), 3.21 – 3.13 (m, 1H, $OCH_bCH_2CH_2N_3$), 3.08 – 2.98 (m, 1H, $OCH_2CH_2CH_aNH_2$), 2.97 – 2.85 (m, 1H, $OCH_2CH_2CH_aNH_2$), 2.18 (dd, *J* = 13.0, 5.0 Hz, 1H, H-3$_{eq}$), 1.88 (s, 3H, CH_3CONH), 1.84 – 1.68 (m, 2H, $OCH_2CH_2CH_2N_3$), 1.48 (dd, *J* = 13.1, 11.5 Hz, 1H, H-3$_{ax}$). ^{13}C NMR (125 MHz, D_2O) δ_C: 175.7, 174.6, 100.2, 70.2, 69.9, 68.1, 66.8, 63.3, 61.2, 52.0, 39.9, 38.3, 26.1, 22.0. HRMS m/z calculated for $C_{14}H_{27}N_2O_9$ $[M+H]^+$: 367.1717; found: 367.1707.

Sia-ligand. Sia-6 (121 mg, 0.330 mmol) was dissolved in 3 mL $NaHCO_3$ solution (10 mg/mL), then 4.5 mL chloroform containing thiophosgene (127 µL, 1.65 mmol) was added. The mixture

was stirred vigorously at room temperature for 6 hours. After the reaction was complete, the reaction mixture was diluted with water, and the aqueous layer was extracted three times with chloroform to remove excess thiophosgene. The aqueous layer was collected, dried, and purified using G-10 column, yielding the Sia-ligand (96 mg) with a 68% yield. ^{1}H NMR (500 MHz, D_2O) δ_H: 4.07 – 3.92 (m, 1H, H-4), 3.81 – 3.68 (m, 4H, H-5, H-7, H-8, H-9a), 3.62 (t, *J* = 6.4 Hz, 2H, $OCH_2CH_2CH_2N_3$), 3.58 – 3.50 (m, 2H, $OCH_aCH_2CH_2N_3$, H-9b), 3.42 - 3.47 (m, 1H, H-6), 3.31 – 3.16 (m, 1H, $OCH_bCH_2CH_2N_3$), 2.25 (dd, *J* = 13.0, 5.0 Hz, 1H, H-3_{eq}), 1.94 (s, 3H, CH_3CONH), 1.92 – 1.80 (m, 2H, $OCH_2CH_2CH_2N_3$), 1.52 (dd, *J* = 13.1, 11.4 Hz, 1H, H-3_{ax}). ^{13}C NMR (125 MHz, D_2O) δ_C: 175.4, 174.8, 160.3, 99.9, 70.2, 70.0, 68.3, 66.9, 63.5, 60.1, 52.0, 42.3, 39.9, 28.9, 22.2. HRMS m/z calculated for $C_{15}H_{24}N_2NaO_9S$ $[M+H]^+$: 431.1100; found: 431.1094.

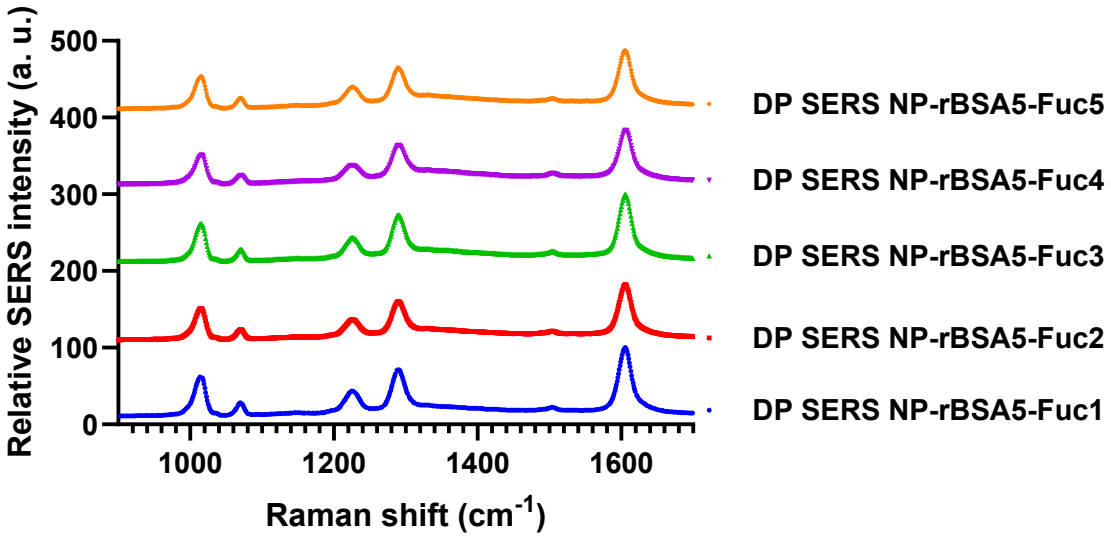

Figure S3. Stacked SERS spectra of 200 pM DP SERS NP–rBSA5–Fuc1–5 plotted in a single axis with vertical offsets to facilitate direct comparison. All spectra were normalized using the intensity of the peak at 1600 cm^{-1} prior to applying vertical offsets. The nearly identical spectral profiles indicate that increasing fucose functionalization does not significantly affect SERS signal intensity up to Fuc5.

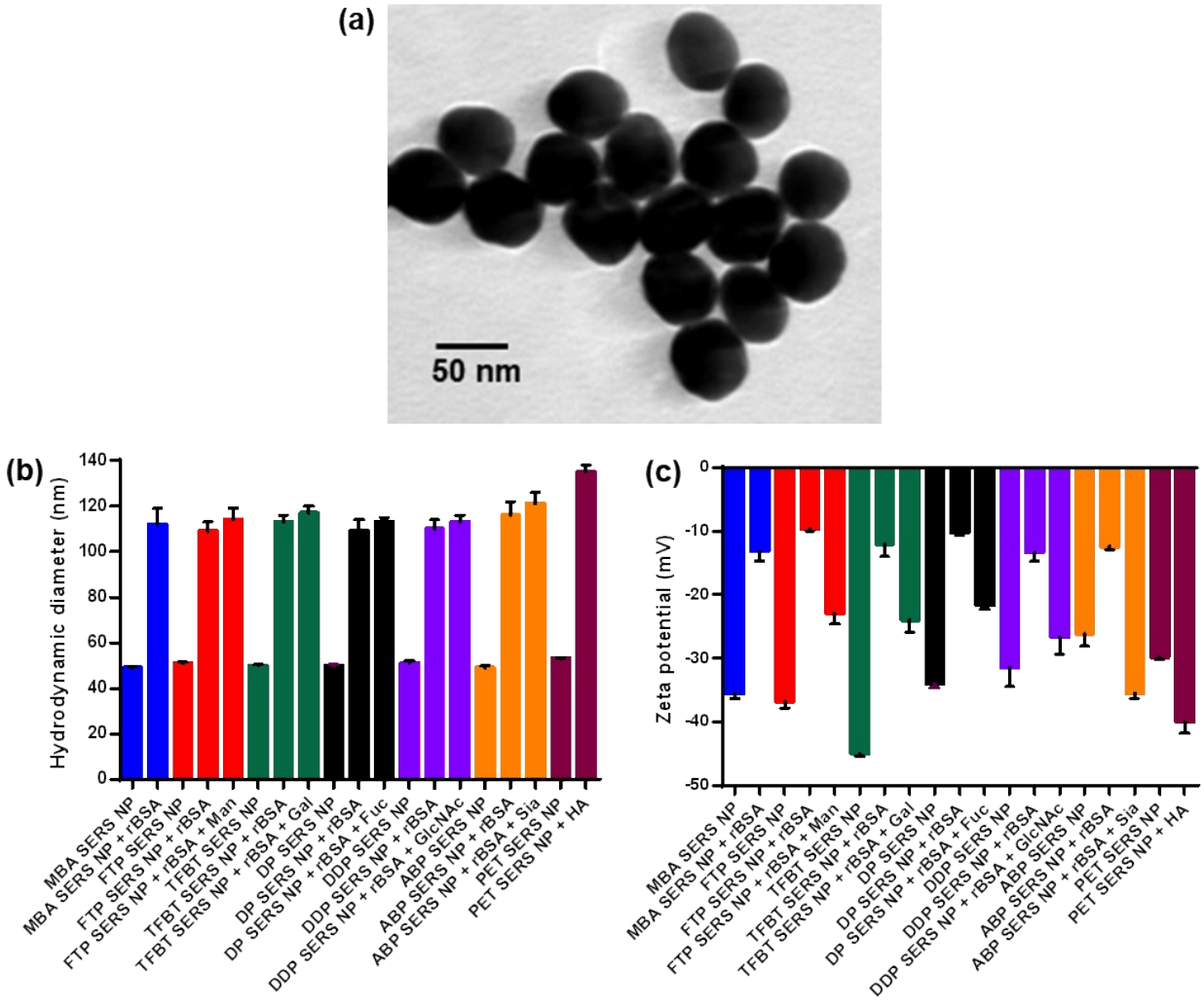

Figure S4. Physicochemical characterization of PlasGlyNPs. (a) TEM image of DP SERS NPs. (b) Hydrodynamic diameter and (i) ζ potential measurements for SERS NPs, SERS NPs+rBSA, and SERS NPs+rBSA+carbohydrates. Data are presented as mean values ± standard deviation, n = 3.

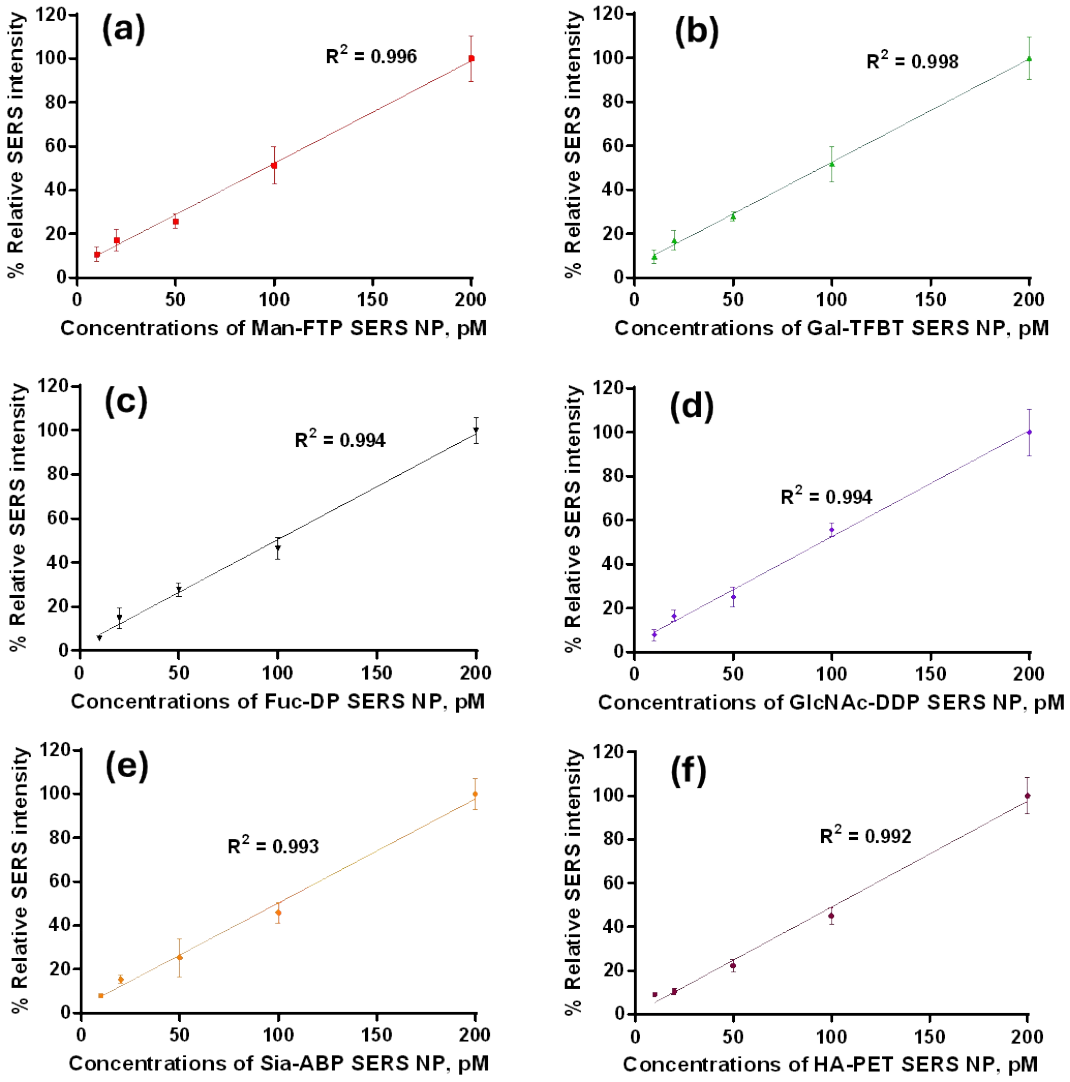

Figure S5. Linearity of PlasGlyNPs: (a) Man-FTP SERS NP, (b) Gal-TFBT SERS NP, (c) Fuc-DP SERS NP, (d) GlcNAc-DDP SERS NP, (e) Sia-ABP SERS NP, and (f) HA-PET SERS NP. Data are presented as mean values ± standard deviation, n = 5. The calibration curves for all the SERS NPs showed excellent linearity, with correlation coefficients (R^2) ranging from 0.992 to 0.998. The concentration of PlasGlyNPs was chosen based on a normalized % relative SERS intensity of 25.

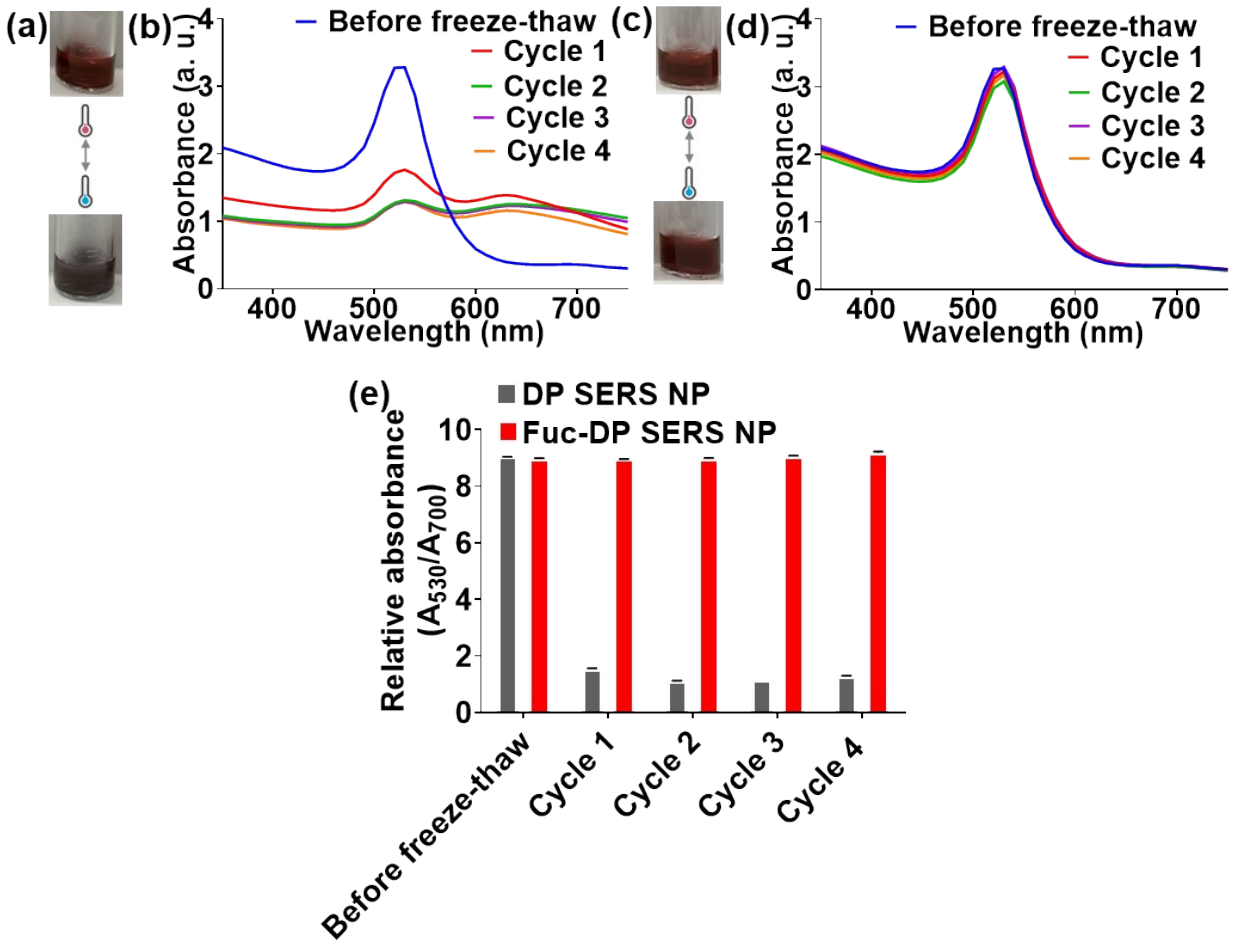

Figure S6. Assessment of aggregation tendency under freeze–thaw for DP SERS NP (without rBSA and carbohydrate functionalization) and Fuc-DP SERS NP (PlasGlyNPs). (a) Photographs of DP SERS NP before and after four freeze–thaw cycles. (b) Plasmonic absorbance spectra of DP SERS NP before and after freeze–thaw cycles. (c) Photographs of Fuc-DP SERS NP before and after four freeze–thaw cycles. (d) Plasmonic absorbance spectra of Fuc-DP SERS NP before and after freeze–thaw cycles. (e) Relative absorbance of DP SERS NP and Fuc-DP SERS NP before and after freeze–thaw cycles. Relative absorbance data are presented as mean values ± standard deviation, n = 3. The results indicate that PlasGlyNPs exhibit superior dispersion stability under freeze–thaw conditions, as evidenced by negligible changes in plasmonic absorbance and absence of visible aggregation.

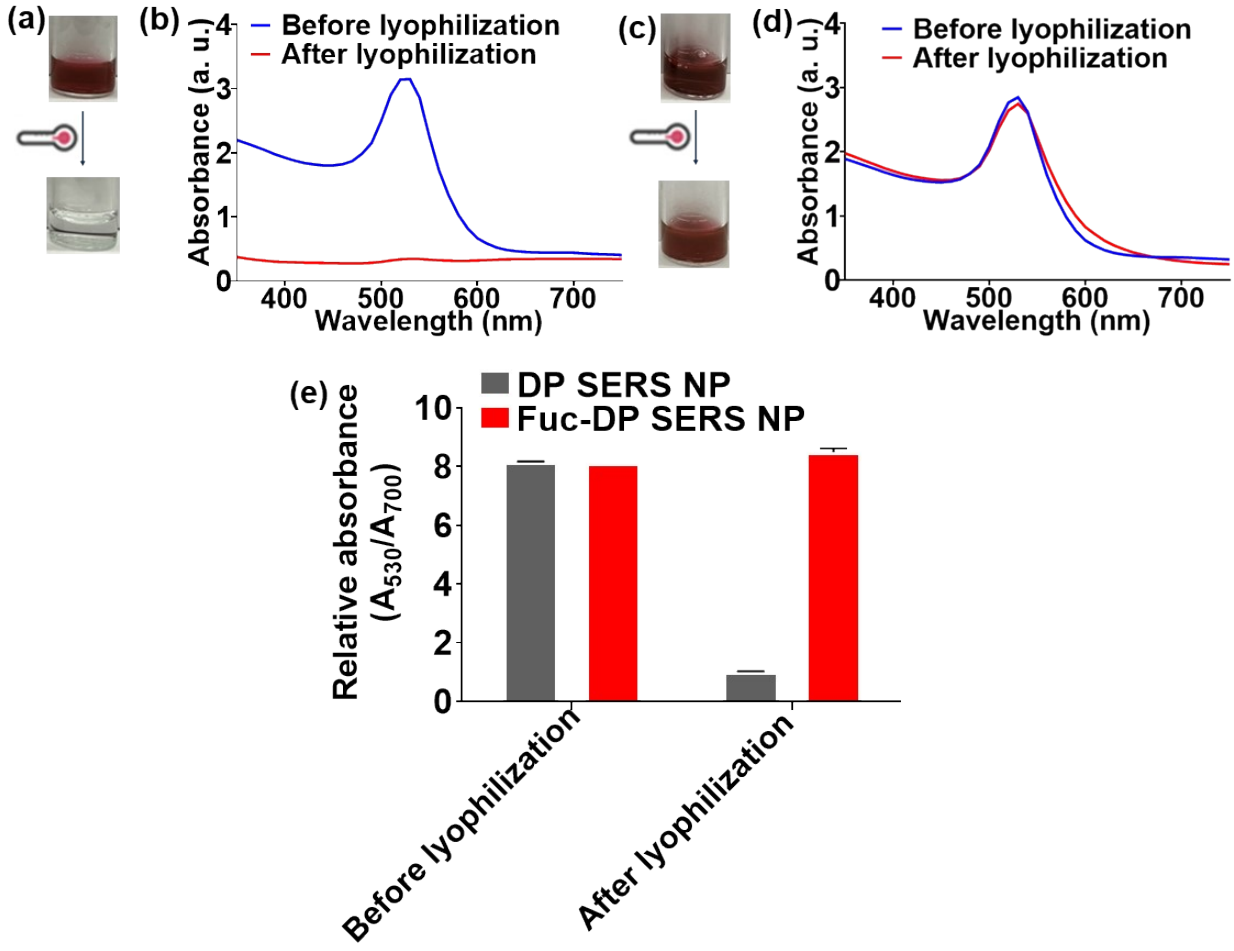

Figure S7. Evaluation of aggregation tendency under lyophilization stress for DP SERS NP (without rBSA and carbohydrate functionalization) and Fuc-DP SERS NP (PlasGlyNPs). (a) Photographs of DP SERS NP before and after lyophilization. (b) Plasmonic absorbance spectra of DP SERS NP before and after lyophilization. (c) Photographs of Fuc-DP SERS NP before and after lyophilization. (d) Plasmonic absorbance spectra of Fuc-DP SERS NP before and after lyophilization. (e) Relative absorbance of DP SERS NP and Fuc-DP SERS NP before and after lyophilization. Relative absorbance data are presented as mean values ± standard deviation, n = 3. These results demonstrate that PlasGlyNPs maintain superior dispersion stability under lyophilization conditions, as indicated by minimal changes in plasmonic absorbance and the absence of visible aggregation.

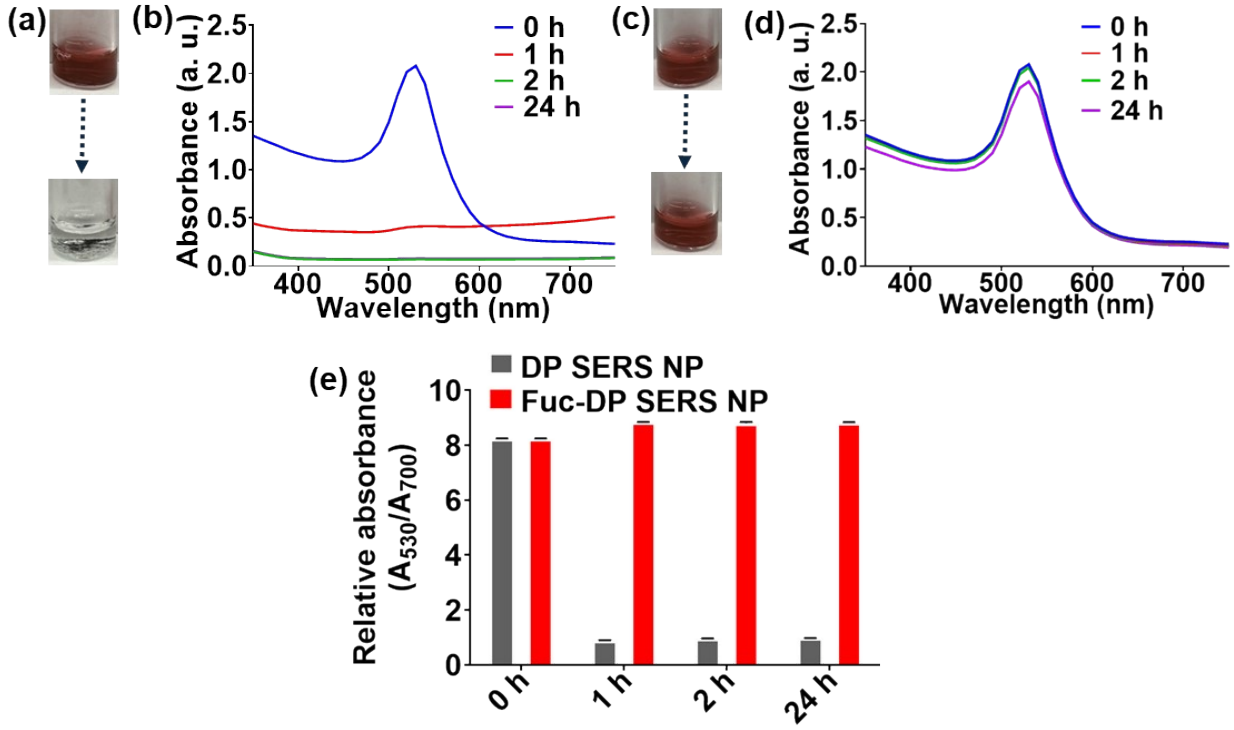

Figure S8. Assessment of aggregation tendency under physiological stress for DP SERS NP (without rBSA and carbohydrate functionalization) and Fuc-DP SERS NP (PlasGlyNPs). (a) Photographs of DP SERS NP in the absence of PBS and after 24 hours in PBS. (b) Plasmonic absorbance spectra of DP SERS NP in the absence of PBS and after 1 hour, 2 hours, and 24 hours in PBS. (c) Photographs of Fuc-DP SERS NP in the absence of PBS and after 24 hours in PBS. (d) Plasmonic absorbance spectra of Fuc-DP SERS NP in the absence of PBS and after 1 hour, 2 hours, and 24 hours in PBS. (e) Relative absorbance of DP SERS NP and Fuc-DP SERS NP in the absence of PBS and after 1 hour, 2 hours, and 24 hours in PBS. Relative absorbance data are presented as mean values ± standard deviation, n = 3. These results demonstrate that PlasGlyNPs exhibit superior dispersion stability under physiological conditions, as evidenced by negligible changes in plasmonic absorbance and the absence of visible aggregation.

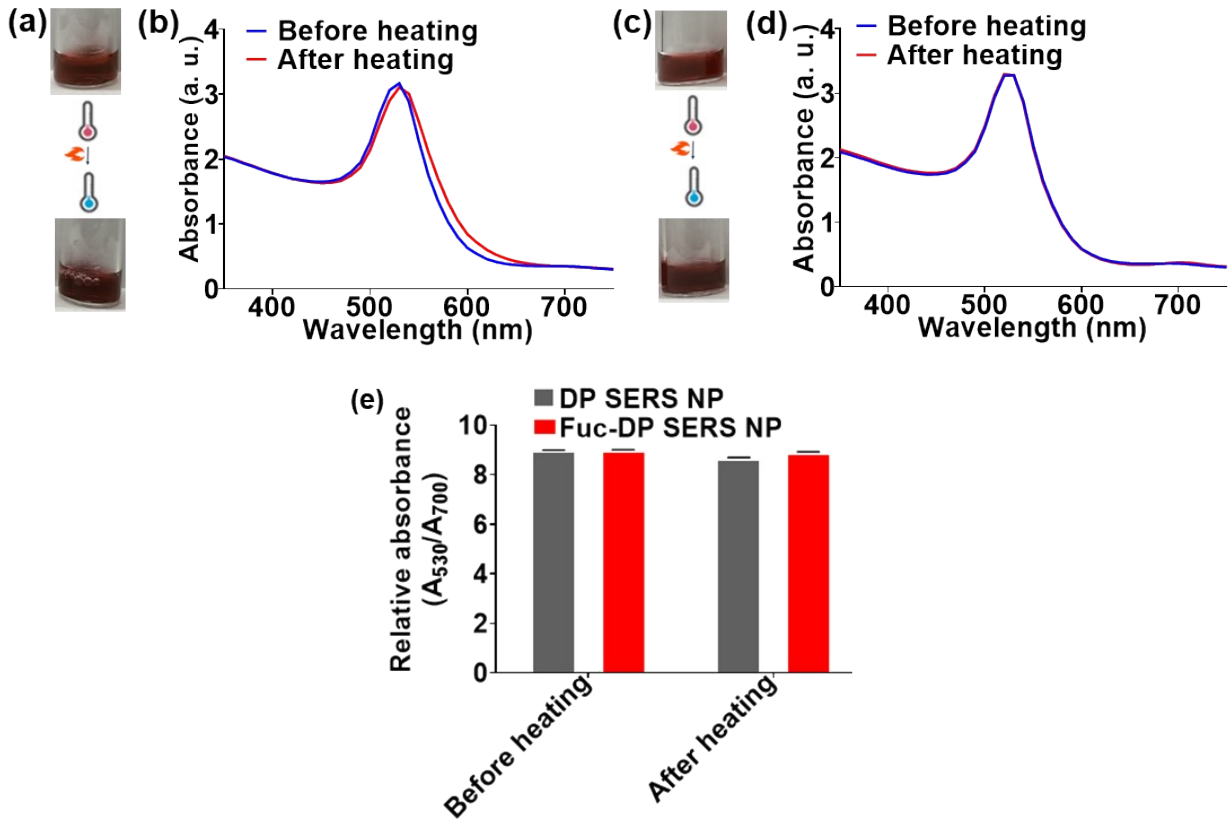

Figure S9. Assessment of aggregation tendency under heating stress for DP SERS NP (without rBSA and carbohydrate functionalization) and Fuc-DP SERS NP (PlasGlyNPs). (a) Photographs of DP SERS NP before and after heating at 85 °C for 4 hours. (b) Plasmonic absorbance spectra of DP SERS NP before and after heating at 85 °C for 4 hours. (c) Photographs of Fuc-DP SERS NP before and after heating at 85 °C for 4 hours. (d) Plasmonic absorbance spectra of Fuc-DP SERS NP before and after heating at 85 °C for 4 hours. (e) Relative absorbance of DP SERS NP and Fuc-DP SERS NP before and after heating at 85 °C for 4 hours. Relative absorbance data are presented as mean values ± standard deviation, n = 3. These results demonstrate that PlasGlyNPs exhibit superior dispersion stability under heating conditions, as evidenced by negligible changes in plasmonic absorbance and the absence of visible aggregation.

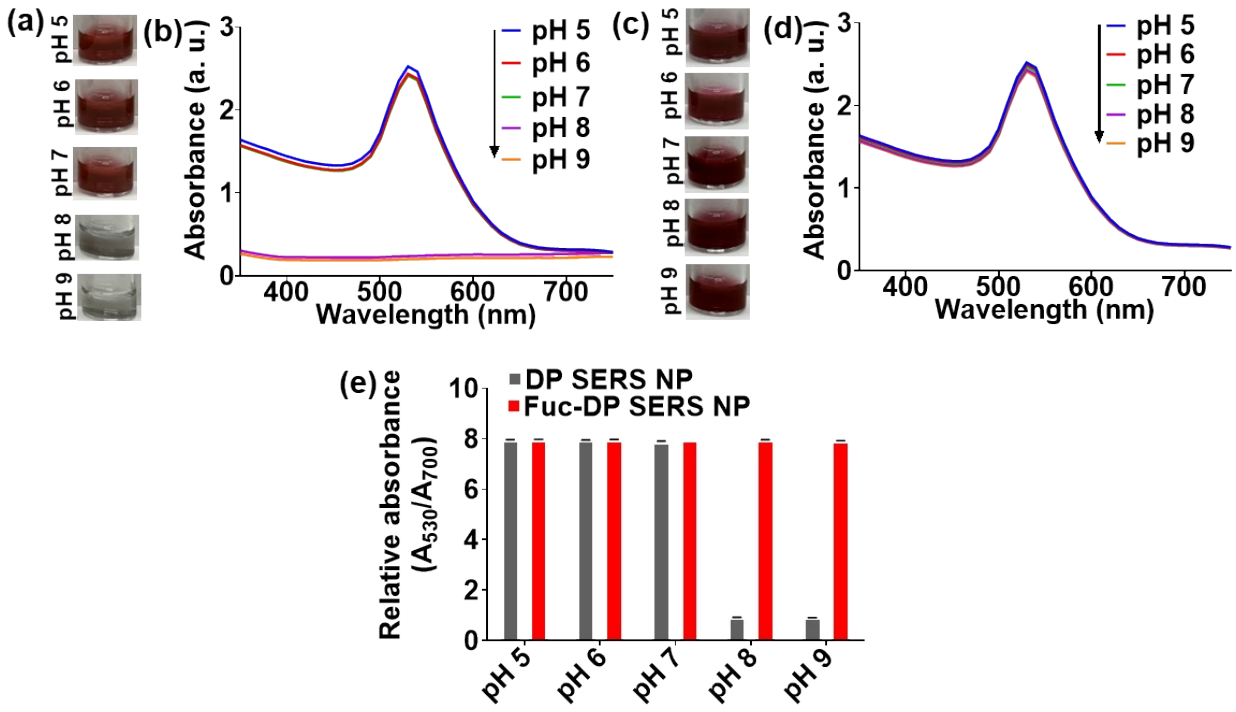

Figure S10. Stability of DP SERS NP (without rBSA or carbohydrate functionalization) and Fuc-DP SERS NP (PlasGlyNPs) under pH stress conditions. (a) Photographs of DP SERS NP at different pH values showing visible aggregation at extreme conditions. (b) Plasmonic absorbance spectra of DP SERS NP under different pH conditions, displaying pronounced peak intensity loss at high pH. (c) Photographs of PlasGlyNPs at different pH values, showing no visible aggregation across the tested range. (d) Plasmonic absorbance spectra of PlasGlyNPs under different pH conditions, demonstrating negligible changes in peak position, shape, and intensity. (e) Relative absorbance comparison of DP SERS NP and PlasGlyNPs across different pH conditions. Relative absorbance data are presented as mean values ± standard deviation, n = 3. Collectively, these results indicate that PlasGlyNPs exhibit markedly improved colloidal stability over a wide pH range, maintaining consistent plasmonic properties and resisting aggregation.

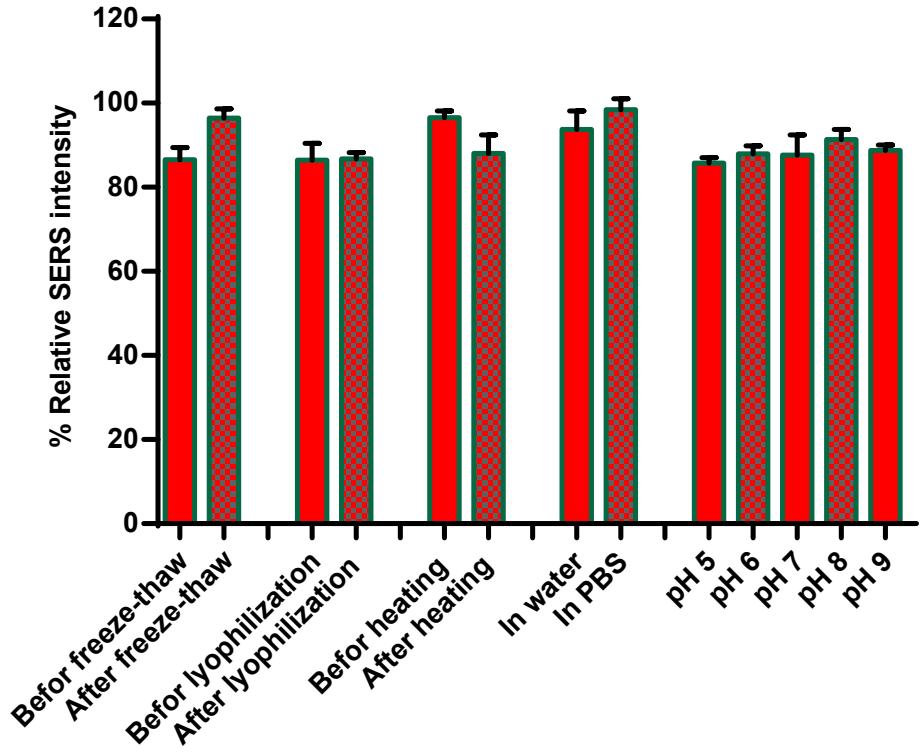

Figure S11. Stability evaluation of PlasGlyNPs under diverse physical and chemical stress conditions. SERS intensity was measured before and after freeze–thaw cycles, lyophilization, and heating at 85 °C, as well as during incubation in water, PBS, and across a range of pH conditions (5–9). Data are presented as mean values ± standard deviation, n = 5. Minimal variations in SERS intensity were observed, confirming that PlasGlyNPs retain their structural integrity and plasmonic properties under these stressors. These results underscore the robustness of PlasGlyNPs and their potential for reliable biosensing and diagnostic applications in challenging environmental and physiological settings.

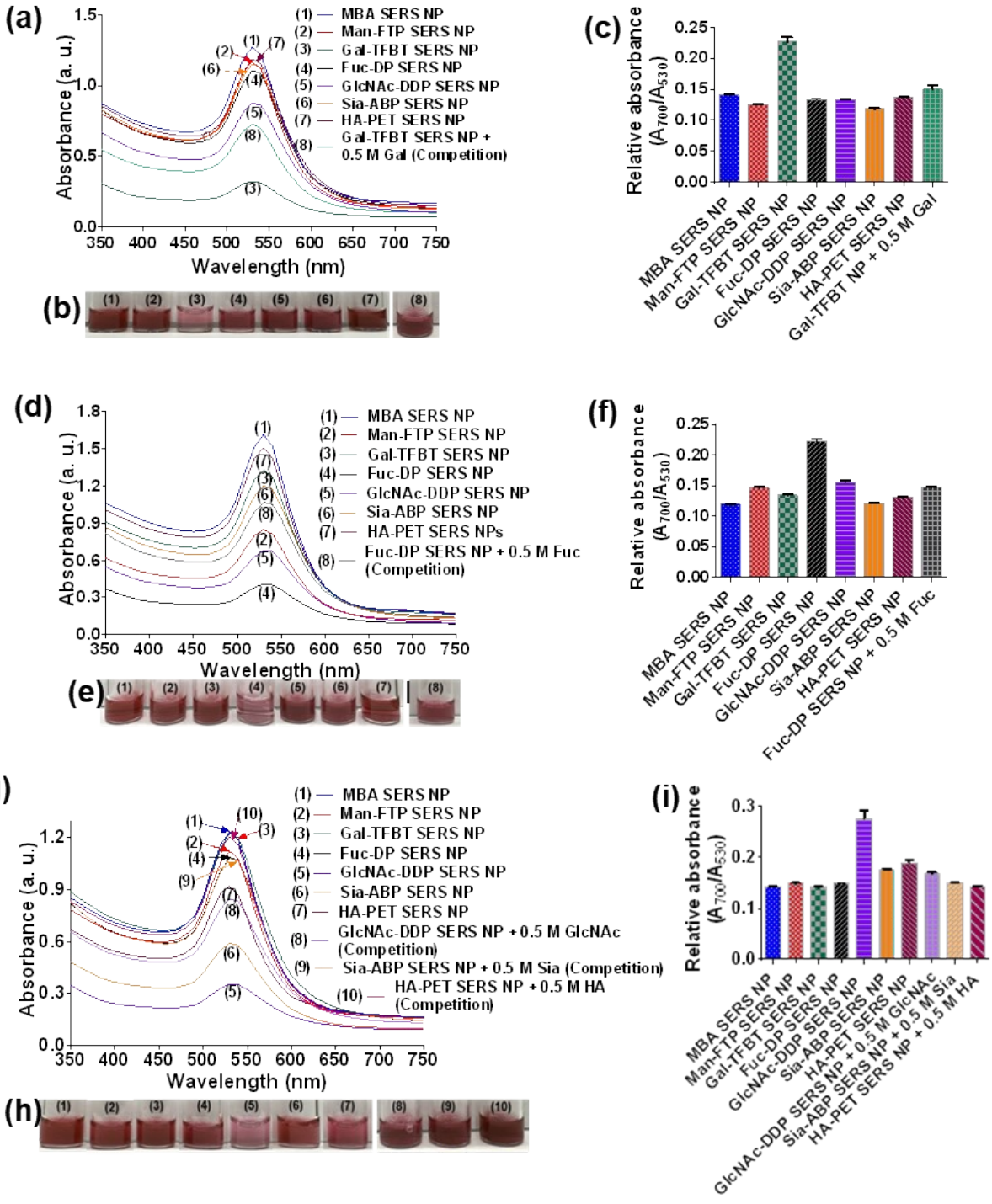

Figure S12. Plasmonic absorption spectra of PlasGlyNPs after incubation with (a) BS-I (20 μg/mL), (d) TPA (20 μg/mL), and (g) WGA (20 μg/mL). Images captured by camera are shown in (b), (e), and (h); and their respective relative absorbance values are presented in (c), (f), and (i). Relative absorbance data are presented as mean values ± standard deviation, n = 3. Gal-TFBT SERS NP bound strongly to Gal-selective BS-I, Fuc-DP SERS NP bound strongly to Fuc-selective TPA, and GlcNAc-DDP SERS NP, Sia-ABP SERS NP, and HA-PET SERS NP bound strongly to GlcNAc- and Sia-selective WGA. Little cross-reactive bindings were observed with non-selective lectins. The binding between lectins and specific PlasGlyNPs could be competitively inhibited using a concentrated solution of the corresponding carbohydrate.

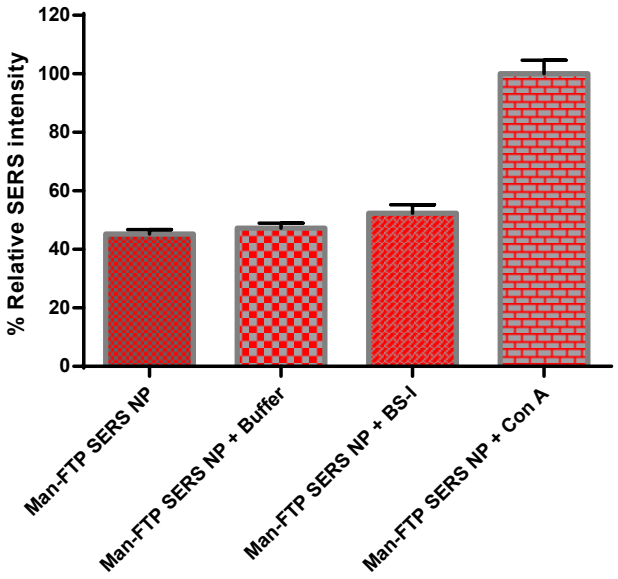

Figure S13. Binding selectivity evaluation of Man-FTP SERS NP. Man-FTP SERS NP was incubated with buffer, BS-I, and Con A respectively and the corresponding Raman spectra were acquired. Data are presented as mean values ± standard deviation, n = 5. A noticeable increase in SERS intensity was observed only in the presence of Con A, demonstrating the selective binding of Man-FTP SERS NP to Con A and confirming the SERS signal enhancement resulted from specific binding interactions.

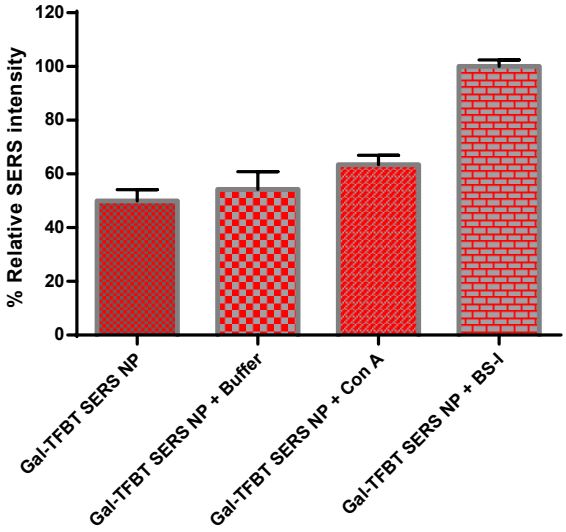

Figure S14. Binding selectivity evaluation of Gal-TFBT SERS NP. Gal-TFBT SERS NP was incubated with buffer, BS-I, and Con A respectively and the Raman spectra were acquired. Data are presented as mean values ± standard deviation, n = 5. A noticeable increase in SERS intensity was only observed in the presence of BS-I, demonstrating selective binding of Gal-TFBT SERS NP to BS-I and confirming the specificity of galactose-lectin interactions.

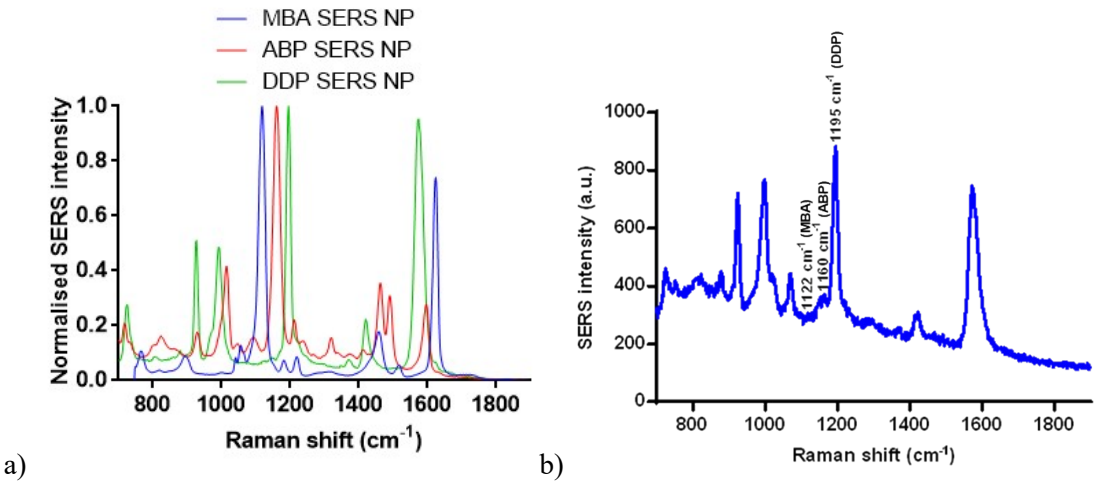

Figure S15. Narrow band width of Raman enabled clear distinction of Raman bands from multiple probes. a) Raman spectra of MBA; ABP and DDP SERS NP. The full width at half maximum of the Raman bands are 14-20 cm^{-1}. Thus, characteristic reporter bands such as those at 1160 cm^{-1} (ABP) and 1195 cm^{-1} (DDP) are clearly distinguishable. B) Mixed SERS spectra recorded from SKOV-3 cells following incubation with the full PlasGlyNP array. SKOV-3 cells bound GlcNAc-DDP SERS NP strongest leading to the highest signal at 1195 cm^{-1} (DDP), while the binding to Sia-ABP SERS NP was much weaker with low signals at 1160 cm-1 (ABP). No significant signal is observed at 1122 cm^{-1} corresponding to the control MBA SERS NP, confirming minimal spectral interference among closely spaced Raman bands.

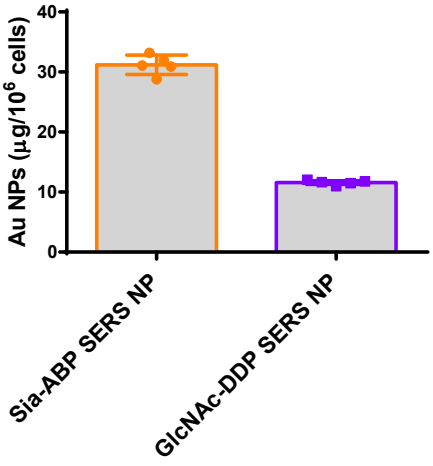

Figure S16. ICP-OES quantification of SERS NP association with MCF7 cells. MCF7 cells were incubated under identical conditions with the high-binding Sia-ABP SERS NPs and the low-binding GlcNAc-DDP SERS NPs, followed by extensive washing to remove unbound particles. The cellular gold content was quantified by ICP-OES. Bars represent mean values with standard deviation of five samples (n = 5). Significantly higher gold uptake was observed for Sia-ABP SERS NP treated cells compared to GlcNAc-DDP SERS NP treated cells, consistent with the relative binding trends observed from SERS signals.

Table S2. Validation of the robustness of the classification model using leave-one-out cross-validation (prediction group analysis). The results demonstrate 100% accuracy for both the original and cross-validated cases, highlighting the reliability and robustness of the LDA model in classifying the data.

Classification Results[a,c]

			Predicted Group Membership									
Cell Line			MCF10A	MCF7	MDA-MB-231	Capan-2	IMR-32	HepG2	HL-60	MC38M1	A549	HeLa
Original	Count	MCF10A	10	0	0	0	0	0	0	0	0	0
		MCF7	0	10	0	0	0	0	0	0	0	0
		MDA-MB-231	0	0	10	0	0	0	0	0	0	0
		Capan-2	0	0	0	10	0	0	0	0	0	0
		IMR-32	0	0	0	0	10	0	0	0	0	0
		HepG2	0	0	0	0	0	10	0	0	0	0
		HL-60	0	0	0	0	0	0	10	0	0	0
		MC38M1	0	0	0	0	0	0	0	10	0	0
		A549	0	0	0	0	0	0	0	0	10	0
		HeLa	0	0	0	0	0	0	0	0	0	10
		SK-MEL-28	0	0	0	0	0	0	0	0	0	0
		SKOV-3	0	0	0	0	0	0	0	0	0	0
	%	MCF10A	100.0	0.0	0.0	0.0	0.0	0.0	0.0	0.0	0.0	0.0
		MCF7	0.0	100.0	0.0	0.0	0.0	0.0	0.0	0.0	0.0	0.0
		MDA-MB-231	0.0	0.0	100.0	0.0	0.0	0.0	0.0	0.0	0.0	0.0
		Capan-2	0.0	0.0	0.0	100.0	0.0	0.0	0.0	0.0	0.0	0.0
		IMR-32	0.0	0.0	0.0	0.0	100.0	0.0	0.0	0.0	0.0	0.0
		HepG2	0.0	0.0	0.0	0.0	0.0	100.0	0.0	0.0	0.0	0.0
		HL-60	0.0	0.0	0.0	0.0	0.0	0.0	100.0	0.0	0.0	0.0
		MC38M1	0.0	0.0	0.0	0.0	0.0	0.0	0.0	100.0	0.0	0.0
		A549	0.0	0.0	0.0	0.0	0.0	0.0	0.0	0.0	100.0	0.0
		HeLa	0.0	0.0	0.0	0.0	0.0	0.0	0.0	0.0	0.0	100.0
		SK-MEL-28	0.0	0.0	0.0	0.0	0.0	0.0	0.0	0.0	0.0	0.0
		SKOV-3	0.0	0.0	0.0	0.0	0.0	0.0	0.0	0.0	0.0	0.0
Cross-validated[b]	Count	MCF10A	10	0	0	0	0	0	0	0	0	0
		MCF7	0	10	0	0	0	0	0	0	0	0
		MDA-MB-231	0	0	10	0	0	0	0	0	0	0
		Capan-2	0	0	0	10	0	0	0	0	0	0
		IMR-32	0	0	0	0	10	0	0	0	0	0
		HepG2	0	0	0	0	0	10	0	0	0	0
		HL-60	0	0	0	0	0	0	10	0	0	0
		MC38M1	0	0	0	0	0	0	0	10	0	0
		A549	0	0	0	0	0	0	0	0	10	0
		HeLa	0	0	0	0	0	0	0	0	0	10
		SK-MEL-28	0	0	0	0	0	0	0	0	0	0
		SKOV-3	0	0	0	0	0	0	0	0	0	0
	%	MCF10A	100.0	0.0	0.0	0.0	0.0	0.0	0.0	0.0	0.0	0.0
		MCF7	0.0	100.0	0.0	0.0	0.0	0.0	0.0	0.0	0.0	0.0
		MDA-MB-231	0.0	0.0	100.0	0.0	0.0	0.0	0.0	0.0	0.0	0.0
		Capan-2	0.0	0.0	0.0	100.0	0.0	0.0	0.0	0.0	0.0	0.0
		IMR-32	0.0	0.0	0.0	0.0	100.0	0.0	0.0	0.0	0.0	0.0
		HepG2	0.0	0.0	0.0	0.0	0.0	100.0	0.0	0.0	0.0	0.0
		HL-60	0.0	0.0	0.0	0.0	0.0	0.0	100.0	0.0	0.0	0.0
		MC38M1	0.0	0.0	0.0	0.0	0.0	0.0	0.0	100.0	0.0	0.0

[a]100.0% of original grouped cases correctly classified.
[b]Cross validation is done only for those cases in the analysis. In cross validation, each case is classified by the functions derived from all cases other than that case.
[c]100.0% of cross-validated grouped cases correctly classified.

Table S3. Confusion matrix for the classification of cell lines using the LDA model. The matrix demonstrates that each cell line was correctly assigned to its respective cluster with 100% accuracy, validating the differentiation power of the SERS signatures.

Classification Results[a]

			Predicted Group Membership										
Cell_Line			MCF10A	MCF7	MDA-MB-231	Capan-2	IMR-32	HepG2	HL-60	MC38M1	A549	HeLa	SK-MEL-28
Original	Count	MCF10A	10	0	0	0	0	0	0	0	0	0	0
		MCF7	0	10	0	0	0	0	0	0	0	0	0
		MDA-MB-231	0	0	10	0	0	0	0	0	0	0	0
		Capan-2	0	0	0	10	0	0	0	0	0	0	0
		IMR-32	0	0	0	0	10	0	0	0	0	0	0
		HepG2	0	0	0	0	0	10	0	0	0	0	0
		HL-60	0	0	0	0	0	0	10	0	0	0	0
		MC38M1	0	0	0	0	0	0	0	10	0	0	0
		A549	0	0	0	0	0	0	0	0	10	0	0
		HeLa	0	0	0	0	0	0	0	0	0	10	0
		SK-MEL-28	0	0	0	0	0	0	0	0	0	0	10
		SKOV-3	0	0	0	0	0	0	0	0	0	0	0
	%	MCF10A	100.0	0.0	0.0	0.0	0.0	0.0	0.0	0.0	0.0	0.0	0.0
		MCF7	0.0	100.0	0.0	0.0	0.0	0.0	0.0	0.0	0.0	0.0	0.0
		MDA-MB-231	0.0	0.0	100.0	0.0	0.0	0.0	0.0	0.0	0.0	0.0	0.0
		Capan-2	0.0	0.0	0.0	100.0	0.0	0.0	0.0	0.0	0.0	0.0	0.0
		IMR-32	0.0	0.0	0.0	0.0	100.0	0.0	0.0	0.0	0.0	0.0	0.0
		HepG2	0.0	0.0	0.0	0.0	0.0	100.0	0.0	0.0	0.0	0.0	0.0
		HL-60	0.0	0.0	0.0	0.0	0.0	0.0	100.0	0.0	0.0	0.0	0.0
		MC38M1	0.0	0.0	0.0	0.0	0.0	0.0	0.0	100.0	0.0	0.0	0.0
		A549	0.0	0.0	0.0	0.0	0.0	0.0	0.0	0.0	100.0	0.0	0.0
		HeLa	0.0	0.0	0.0	0.0	0.0	0.0	0.0	0.0	0.0	100.0	0.0
		SK-MEL-28	0.0	0.0	0.0	0.0	0.0	0.0	0.0	0.0	0.0	0.0	100.0
		SKOV-3	0.0	0.0	0.0	0.0	0.0	0.0	0.0	0.0	0.0	0.0	0.0

a. 100.0% of original grouped cases correctly classified.

Table S4. Wilks' Lambda analysis of discriminant functions in the LDA model. The low Wilks' Lambda values and highly significant Chi-square tests ($p < 0.001$) for each discriminant function confirm their substantial contribution to group separation, reinforcing the robustness and reliability of the LDA results.

Wilks' Lambda

Test of Function(s)	Wilks' Lambda	Chi-square	df	Sig.
1 through 6	0.000	2151.384	66	0.000
2 through 6	0.000	1639.509	50	0.000
3 through 6	0.000	1138.106	36	0.000
4 through 6	0.001	773.508	24	0.000
5 through 6	0.022	418.971	14	0.000
6	0.176	190.933	6	0.000

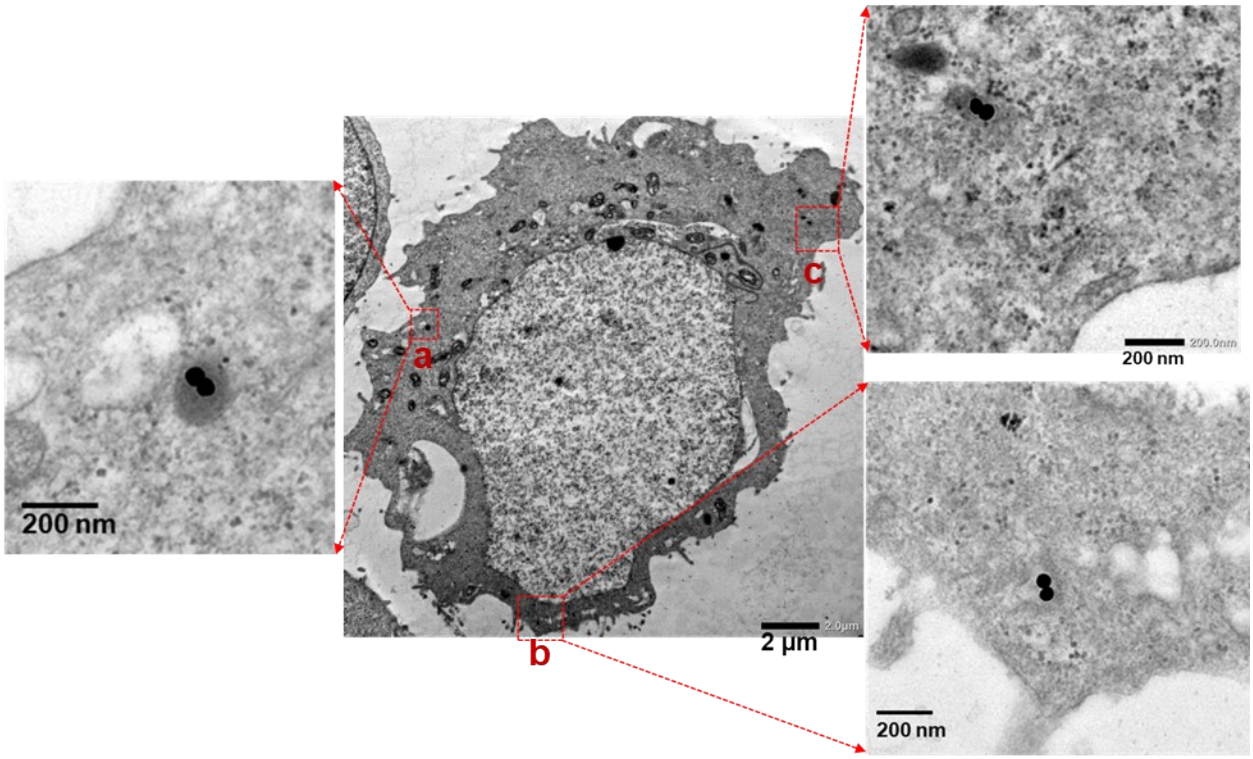

Figure S17. TEM image of an MCF7 cell incubated with Sia-ABP SERS NP, followed by thorough washing to remove unbound particles. The central panel shows the overall cell morphology, while the red-boxed regions (a–c) highlight intracellular compartments containing electron-dense gold nanoparticles. Enlarged views of these regions confirm the localization of nanoparticles within membrane-bound vesicular structures, indicating uptake and vesicular trapping of the glyco-nanoparticles.

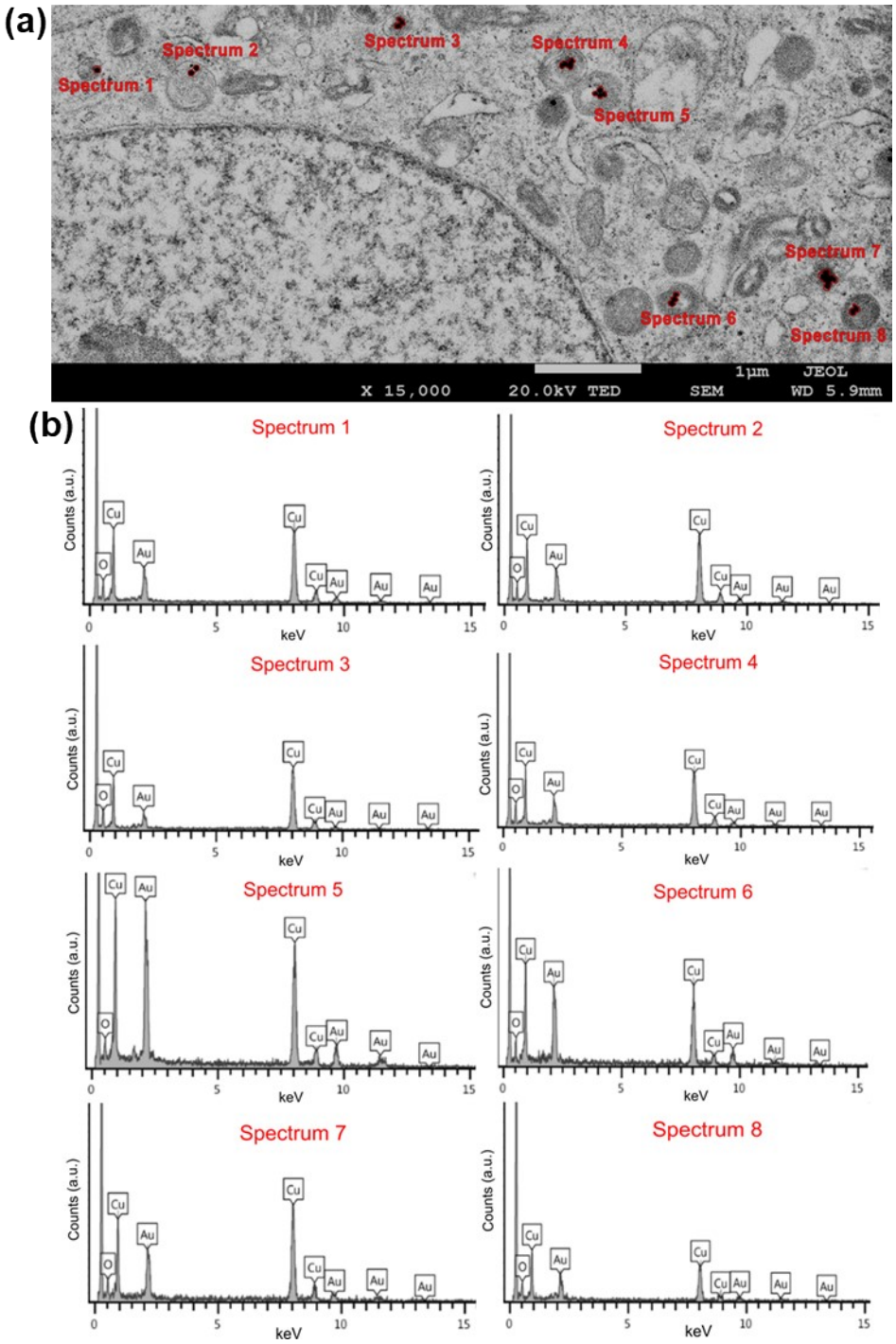

Figure S18. (a) SEM image of an MCF7 cell incubated with Sia-ABP SERS nanoparticles, followed by thorough washing to remove unbound particles. Multiple electron-dense spots are observed within the cell, corresponding to internalized Au (gold) nanoparticles. (b) EDX analysis was performed at eight selected regions (Spectrum 1–8), indicated in red on the SEM image. The corresponding EDX spectra confirm the presence of Au signals at all measured points, verifying intracellular localization of the nanoparticles. These results further support the selective uptake and intracellular presence of Sia-ABP SERS NP in MCF7 cells.

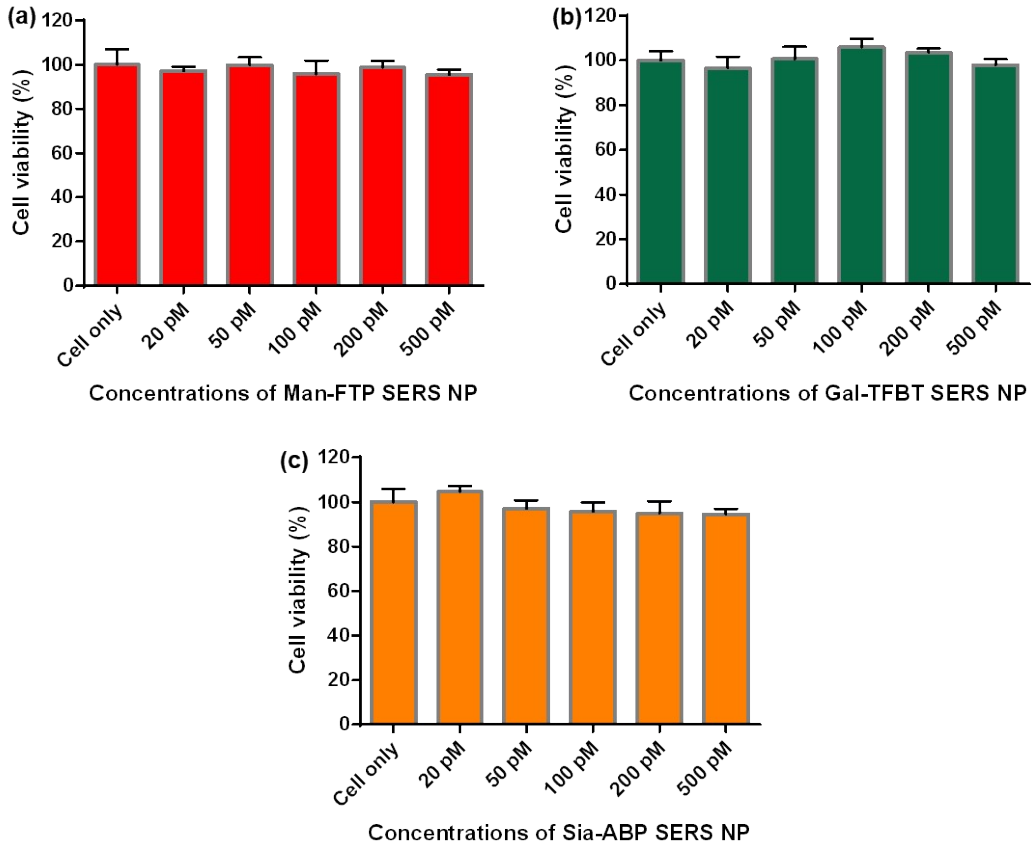

Figure S19. MTS assay of a) MCF10A incubated with Man-FTP SERS NP, b) MDA-MB-231 incubated with Gal-TFBT SERS NP, and (c) HepG2 incubated with Sia-ABP SERS NP showed no toxicity after 6 hour incubation. Data are presented as mean values ± standard deviation, n = 3.

NMR Spectra

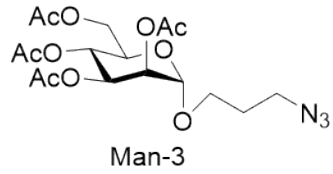

Man-3

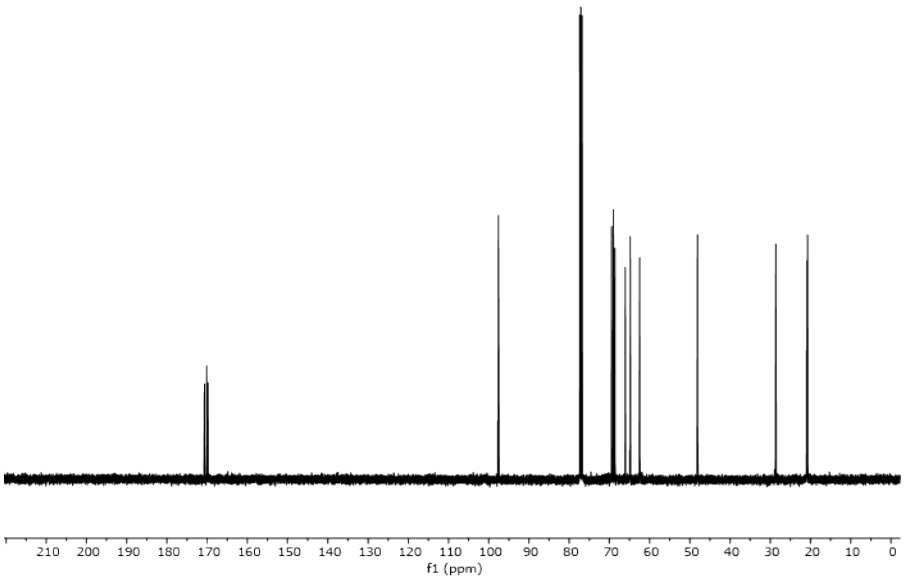

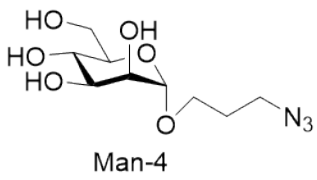
HO
OH
HO
O
HO
O
N3

Man-4

11.0 10.5 10.0 9.5 9.0 8.5 8.0 7.5 7.0 6.5 6.0 5.5 5.0 4.5 4.0 3.5 3.0 2.5 2.0 1.5 1.0 0.5
f1 (ppm)

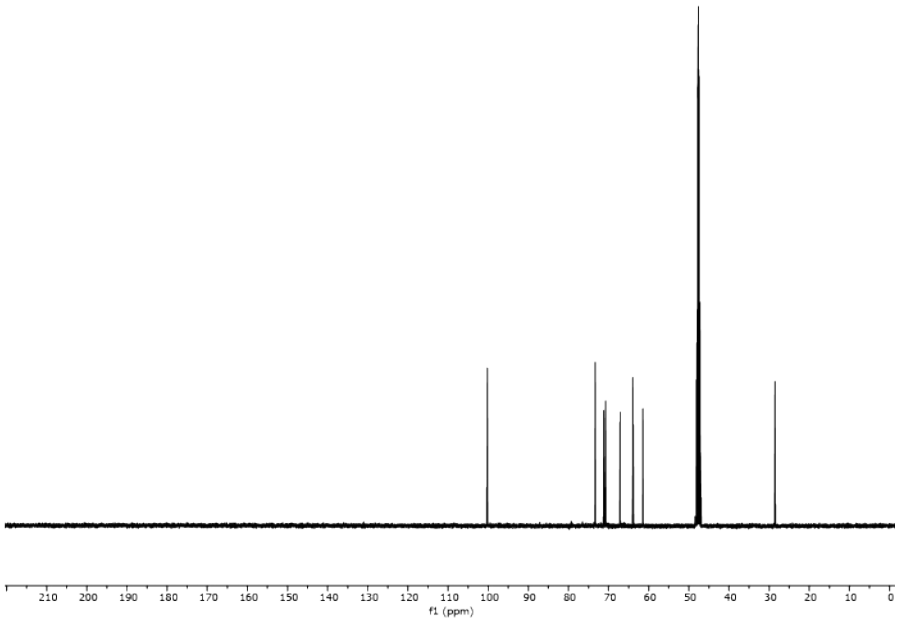
210 200 190 180 170 160 150 140 130 120 110 100 90 80 70 60 50 40 30 20 10 0
f1 (ppm)

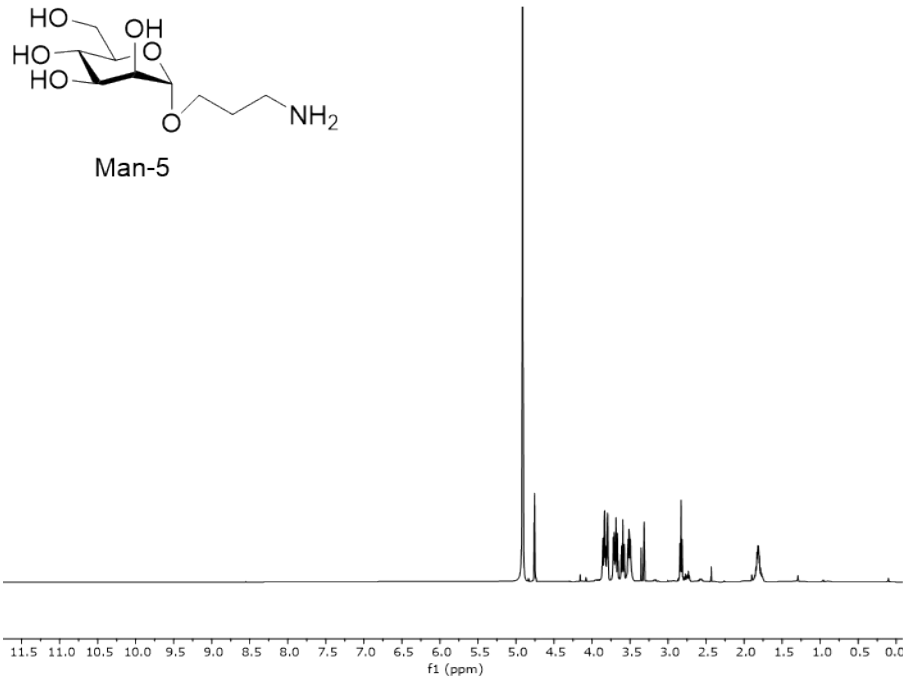
HO
OH
HO
O
HO
O
NH2
11.5 11.0 10.5 10.0 9.5 9.0 8.5 8.0 7.5 7.0 6.5 6.0 5.5 5.0 4.5 4.0 3.5 3.0 2.5 2.0 1.5 1.0 0.5 0.0
f1 (ppm)

Man-5

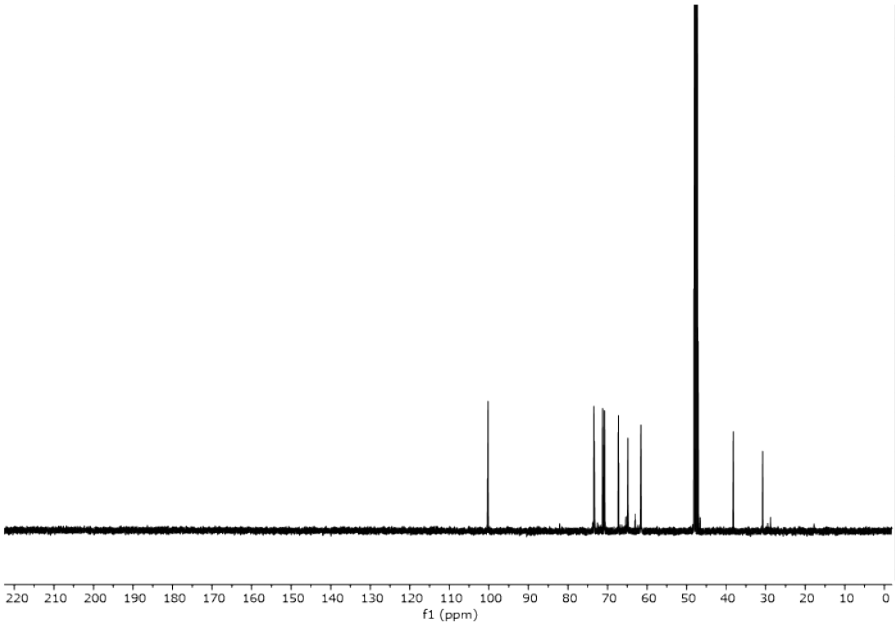
220 210 200 190 180 170 160 150 140 130 120 110 100 90 80 70 60 50 40 30 20 10 0
f1 (ppm)

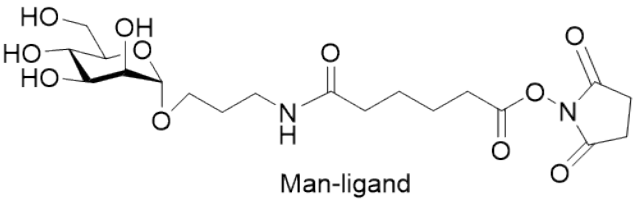
HO
OH
HO
HO
O
O
N
H
O
O
O
N
O
O

Man-ligand

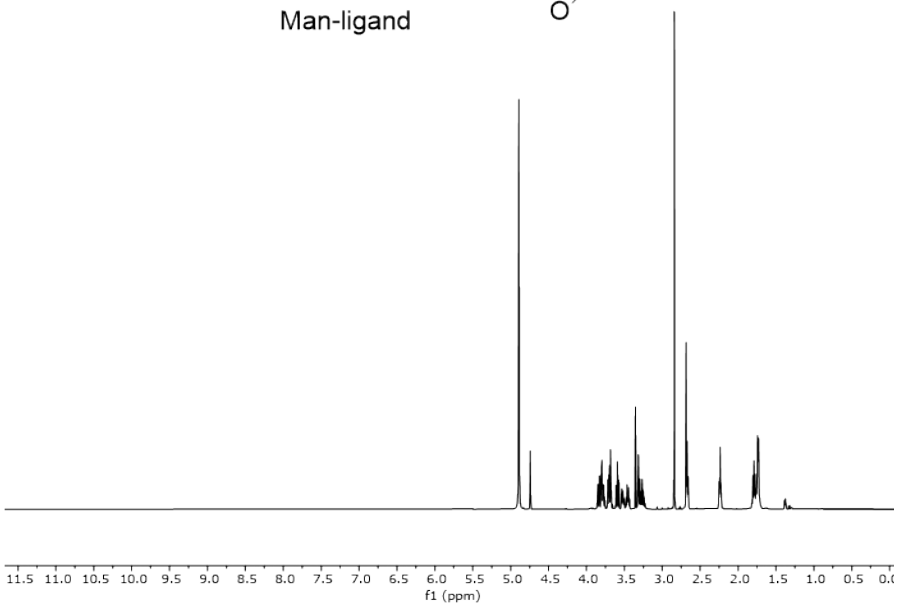
11.5 11.0 10.5 10.0 9.5 9.0 8.5 8.0 7.5 7.0 6.5 6.0 5.5 5.0 4.5 4.0 3.5 3.0 2.5 2.0 1.5 1.0 0.5
f1 (ppm)

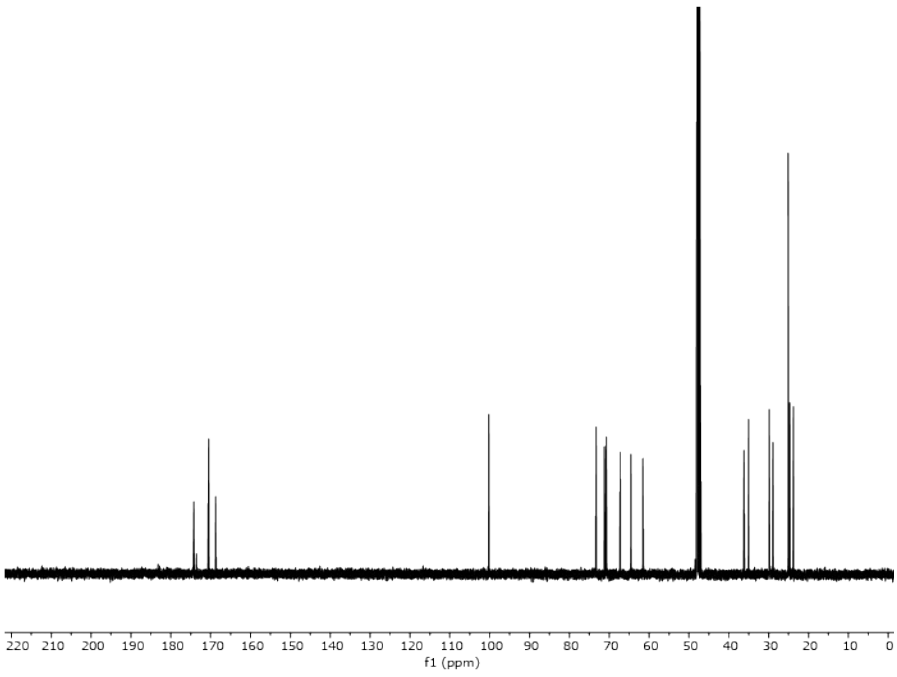
220 210 200 190 180 170 160 150 140 130 120 110 100 90 80 70 60 50 40 30 20 10 0
f1 (ppm)

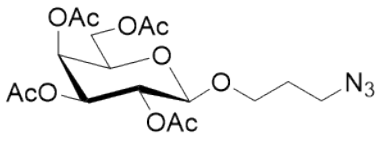
OAc
OAc
O
AcO
O
N3
OAc

Gal-3

11.0 10.5 10.0 9.5 9.0 8.5 8.0 7.5 7.0 6.5 6.0 5.5 5.0 4.5 4.0 3.5 3.0 2.5 2.0 1.5 1.0 0.5
f1 (ppm)

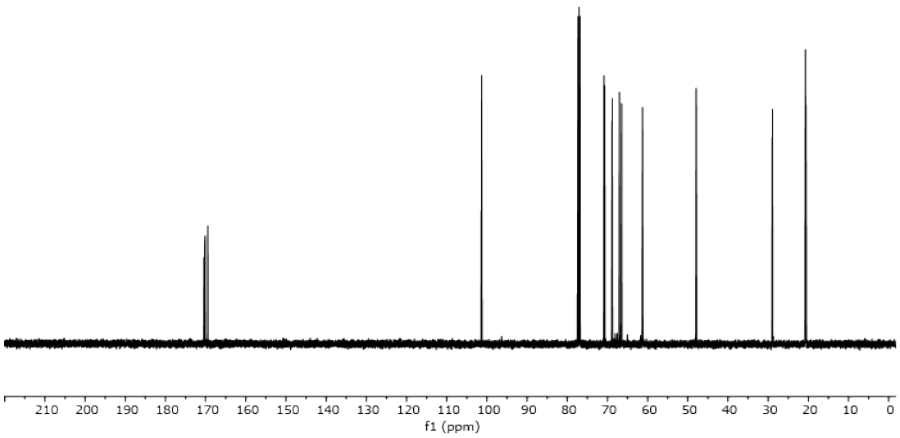
210 200 190 180 170 160 150 140 130 120 110 100 90 80 70 60 50 40 30 20 10 0
f1 (ppm)

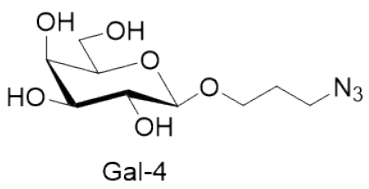
OH
OH
O
HO
O
N3
OH

Gal-4

11.0 10.5 10.0 9.5 9.0 8.5 8.0 7.5 7.0 6.5 6.0 5.5 5.0 4.5 4.0 3.5 3.0 2.5 2.0 1.5 1.0 0.5 0.0
f1 (ppm)

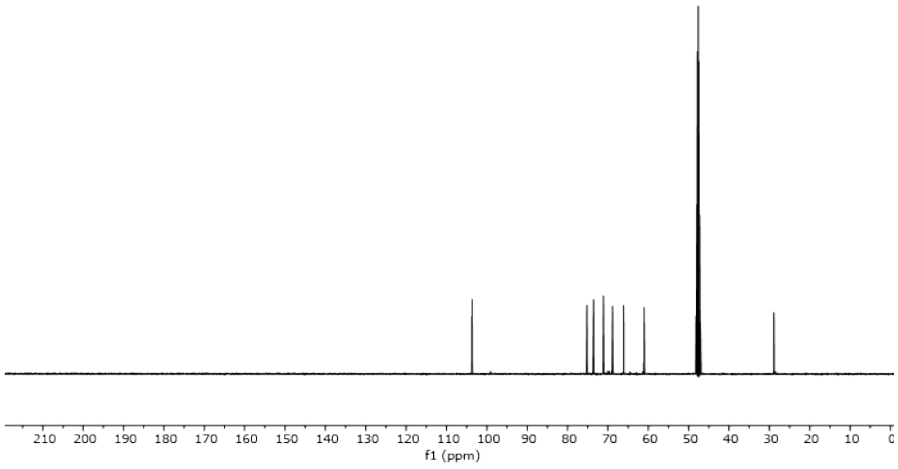
210 200 190 180 170 160 150 140 130 120 110 100 90 80 70 60 50 40 30 20 10 0
f1 (ppm)

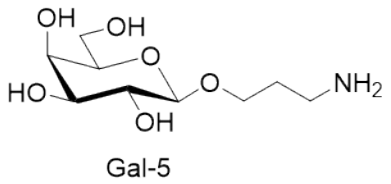
OH
OH
O
HO
O
NH2
OH

Gal-5

11.0 10.5 10.0 9.5 9.0 8.5 8.0 7.5 7.0 6.5 6.0 5.5 5.0 4.5 4.0 3.5 3.0 2.5 2.0 1.5 1.0 0.5
f1 (ppm)

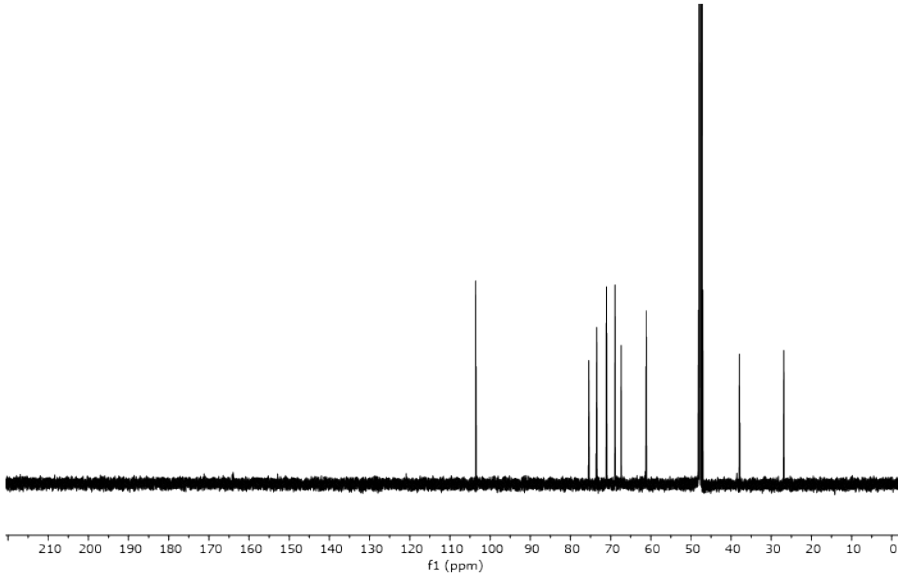
210 200 190 180 170 160 150 140 130 120 110 100 90 80 70 60 50 40 30 20 10 0
f1 (ppm)

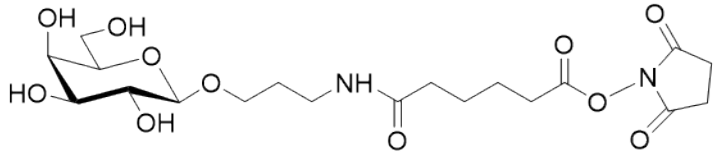
OH
OH
O
HO
OH
O
NH
O
O
O
N
O
O

Gal-ligand

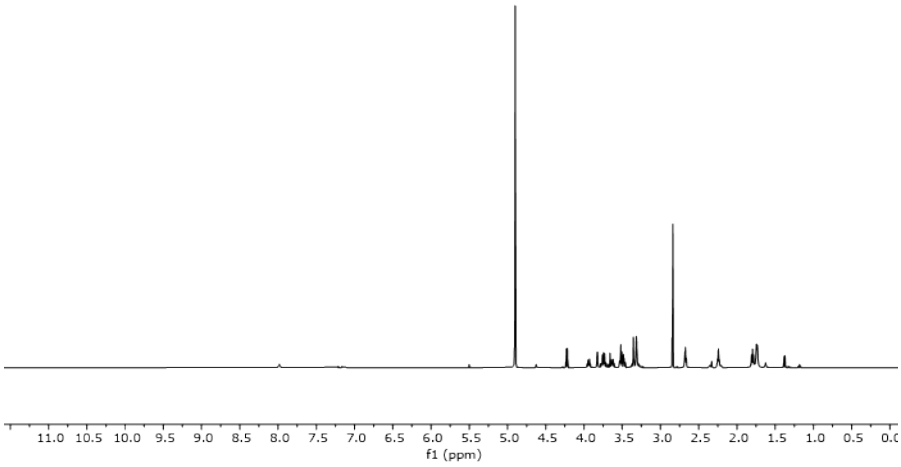
11.0 10.5 10.0 9.5 9.0 8.5 8.0 7.5 7.0 6.5 6.0 5.5 5.0 4.5 4.0 3.5 3.0 2.5 2.0 1.5 1.0 0.5
f1 (ppm)

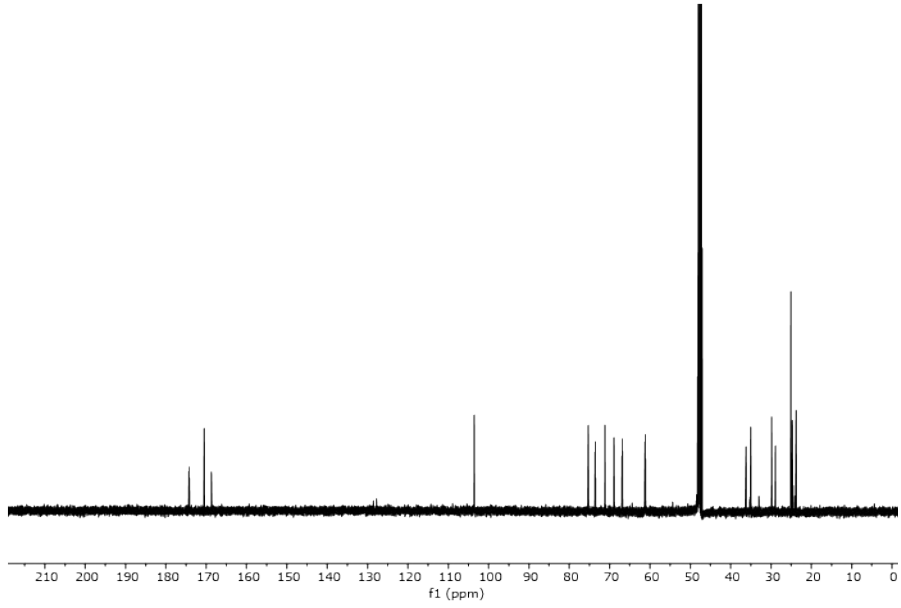
210 200 190 180 170 160 150 140 130 120 110 100 90 80 70 60 50 40 30 20 10 0
f1 (ppm)

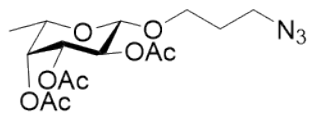
O
O
OAc
OAc
OAc
N3

Fuc-4

11.0 10.5 10.0 9.5 9.0 8.5 8.0 7.5 7.0 6.5 6.0 5.5 5.0 4.5 4.0 3.5 3.0 2.5 2.0 1.5 1.0 0.5 0.0
f1 (ppm)

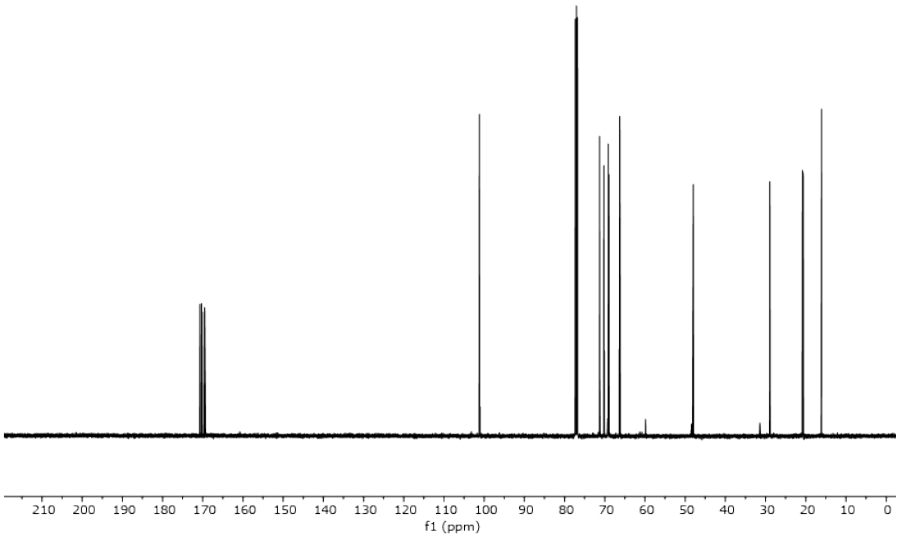
210 200 190 180 170 160 150 140 130 120 110 100 90 80 70 60 50 40 30 20 10 0
f1 (ppm)

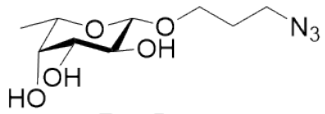
O
O
OH
N3
OH
HO

Fuc-5

11.0 10.5 10.0 9.5 9.0 8.5 8.0 7.5 7.0 6.5 6.0 5.5 5.0 4.5 4.0 3.5 3.0 2.5 2.0 1.5 1.0 0.5
f1 (ppm)

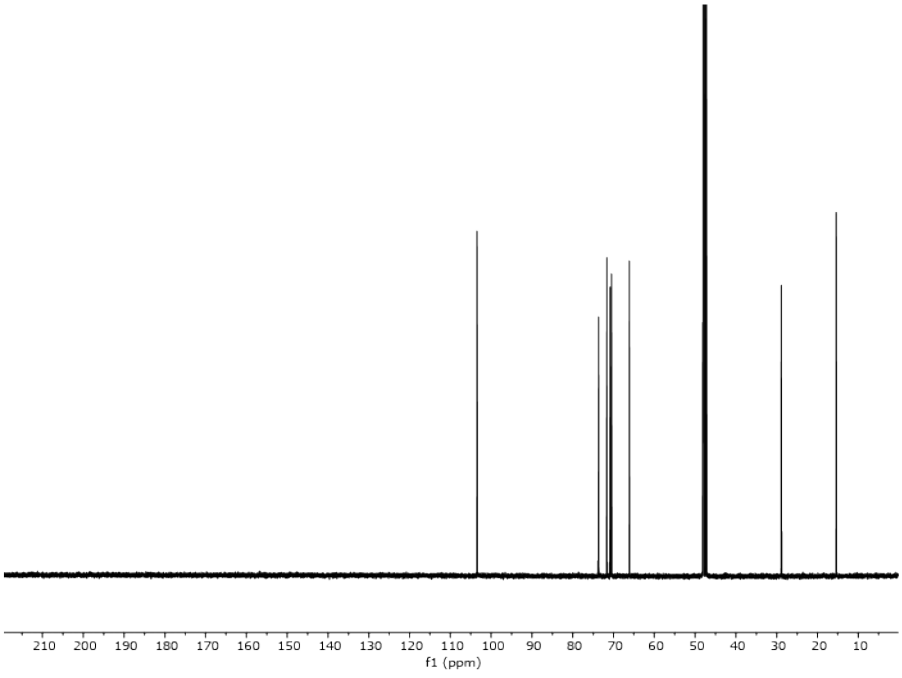
210 200 190 180 170 160 150 140 130 120 110 100 90 80 70 60 50 40 30 20 10
f1 (ppm)

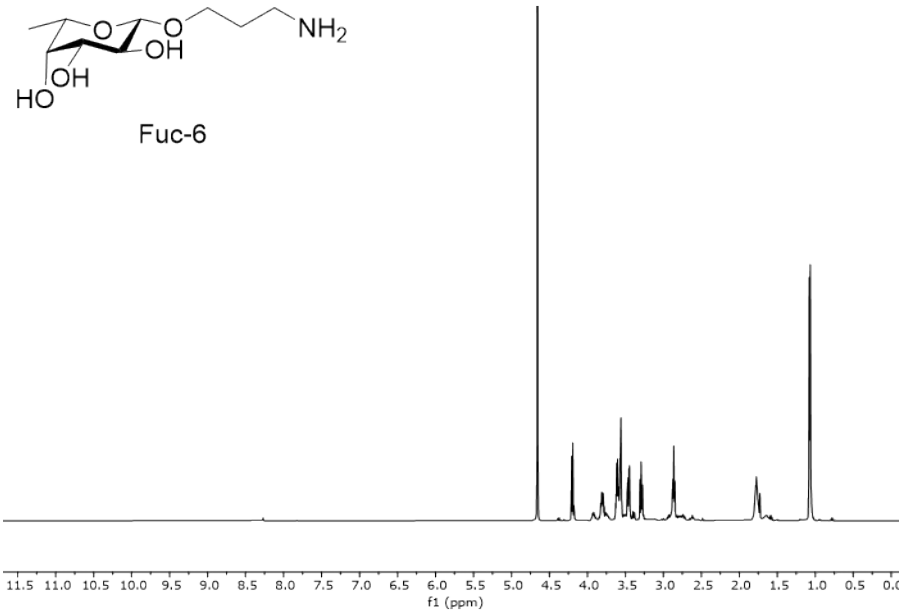
NH2
O
O
OH
OH
HO
11.5 11.0 10.5 10.0 9.5 9.0 8.5 8.0 7.5 7.0 6.5 6.0 5.5 5.0 4.5 4.0 3.5 3.0 2.5 2.0 1.5 1.0 0.5
f1 (ppm)

Fuc-6

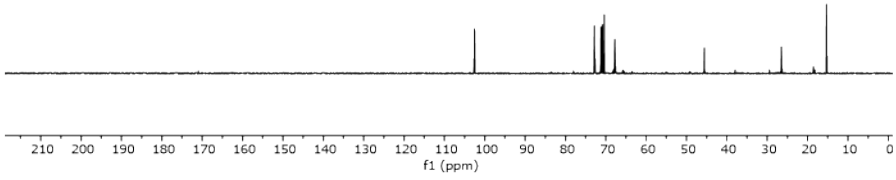
210 200 190 180 170 160 150 140 130 120 110 100 90 80 70 60 50 40 30 20 10 0
f1 (ppm)

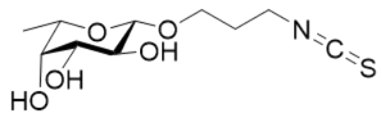
O
O
OH
OH
HO
N
C
S

Fuc-ligand

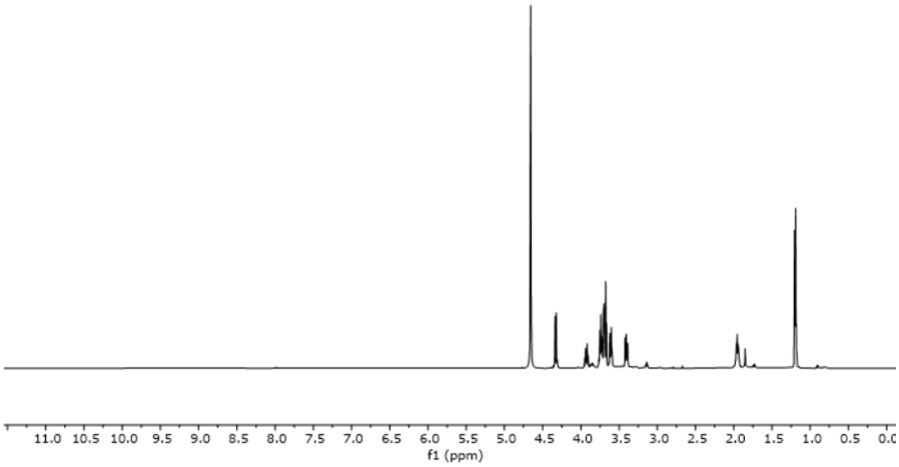
11.0 10.5 10.0 9.5 9.0 8.5 8.0 7.5 7.0 6.5 6.0 5.5 5.0 4.5 4.0 3.5 3.0 2.5 2.0 1.5 1.0 0.5 0.0
f1 (ppm)

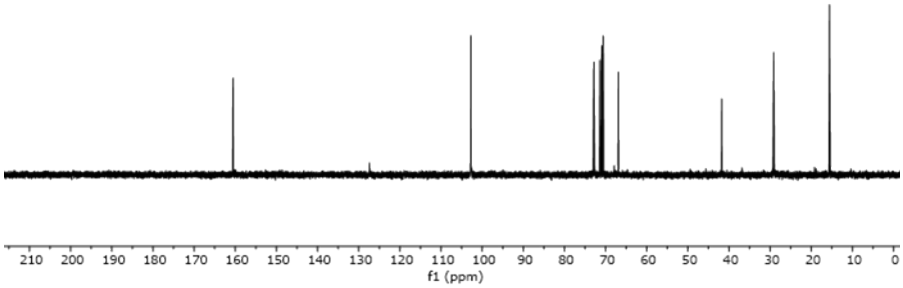
210 200 190 180 170 160 150 140 130 120 110 100 90 80 70 60 50 40 30 20 10 0
f1 (ppm)

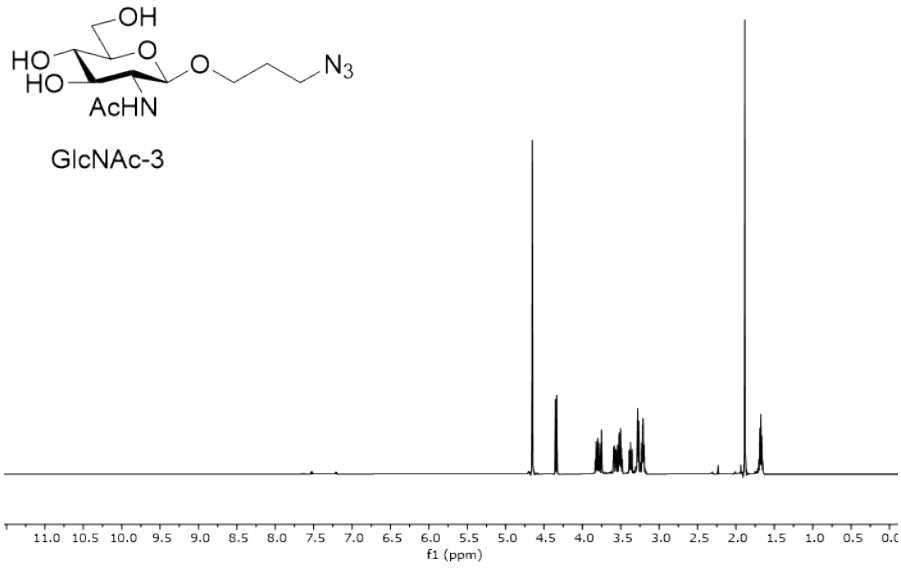
OH
HO
HO
O
O
N3
AcHN
GlcNAc-3
11.0 10.5 10.0 9.5 9.0 8.5 8.0 7.5 7.0 6.5 6.0 5.5 5.0 4.5 4.0 3.5 3.0 2.5 2.0 1.5 1.0 0.5
f1 (ppm)

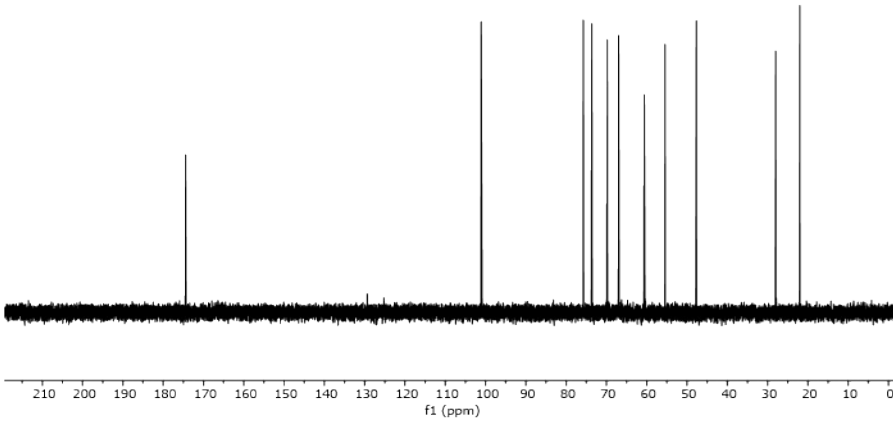
210 200 190 180 170 160 150 140 130 120 110 100 90 80 70 60 50 40 30 20 10
f1 (ppm)

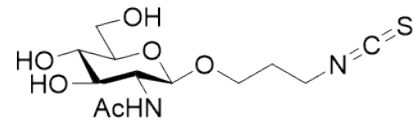

GlcNAc-ligand

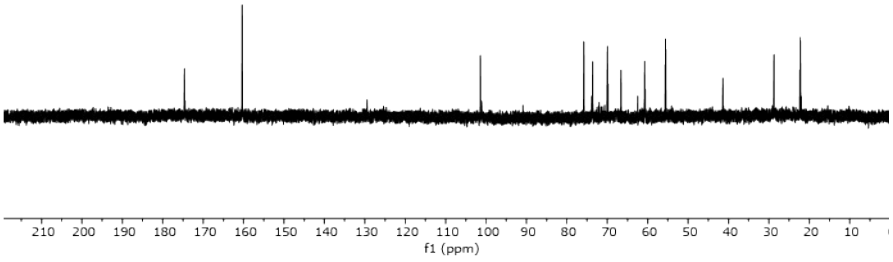

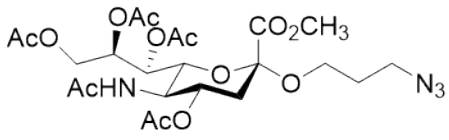
AcO
OAc
OAc
CO2CH3
AcHN
O
O
N3
AcO

Sia-4

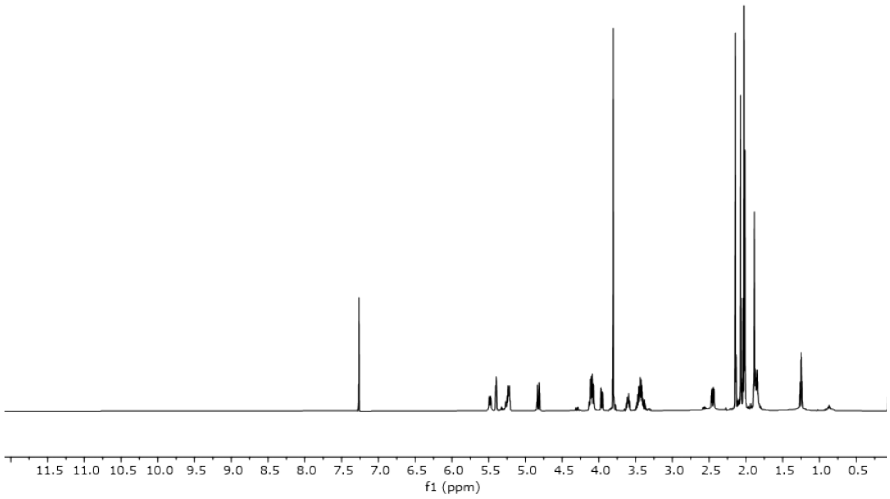
11.5 11.0 10.5 10.0 9.5 9.0 8.5 8.0 7.5 7.0 6.5 6.0 5.5 5.0 4.5 4.0 3.5 3.0 2.5 2.0 1.5 1.0 0.5
f1 (ppm)

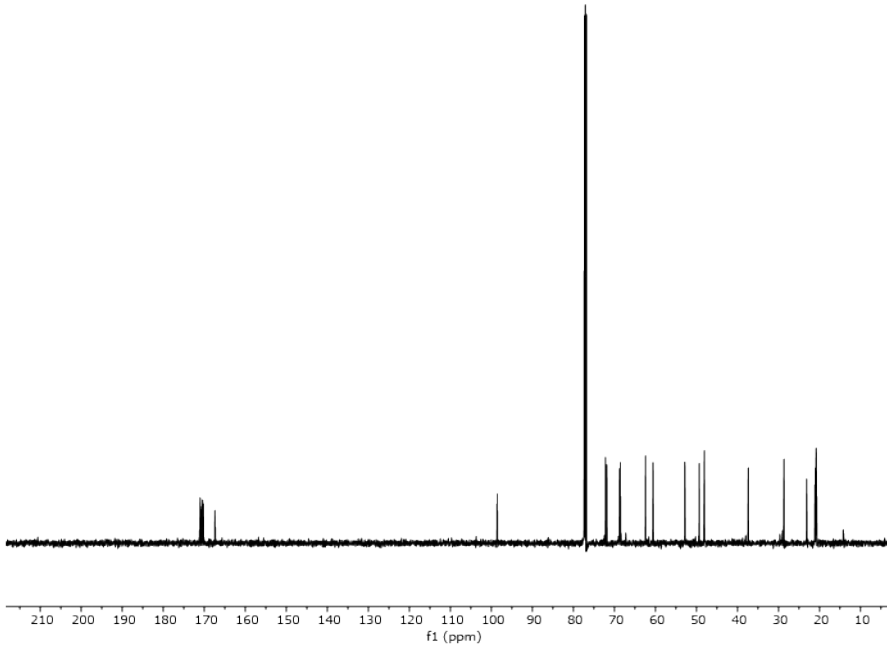
210 200 190 180 170 160 150 140 130 120 110 100 90 80 70 60 50 40 30 20 10
f1 (ppm)

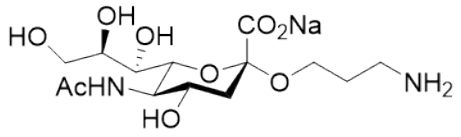
HO
OH
OH
CO2Na
AcHN
O
O
NH2
HO

Sia-6

11.5 11.0 10.5 10.0 9.5 9.0 8.5 8.0 7.5 7.0 6.5 6.0 5.5 5.0 4.5 4.0 3.5 3.0 2.5 2.0 1.5 1.0 0.5
f1 (ppm)

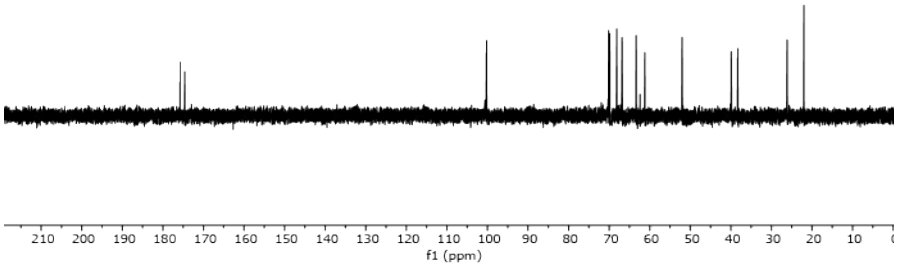
210 200 190 180 170 160 150 140 130 120 110 100 90 80 70 60 50 40 30 20 10
f1 (ppm)

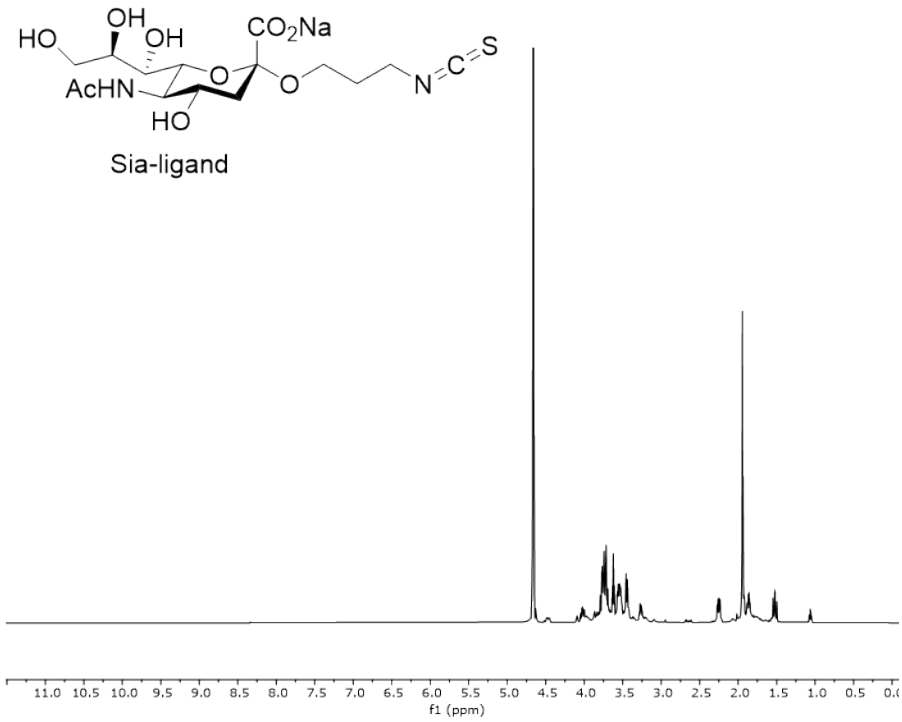
HO
OH
OH
AcHN
HO
O
CO2Na
O
N=C=S
11.0 10.5 10.0 9.5 9.0 8.5 8.0 7.5 7.0 6.5 6.0 5.5 5.0 4.5 4.0 3.5 3.0 2.5 2.0 1.5 1.0 0.5
f1 (ppm)

Sia-ligand

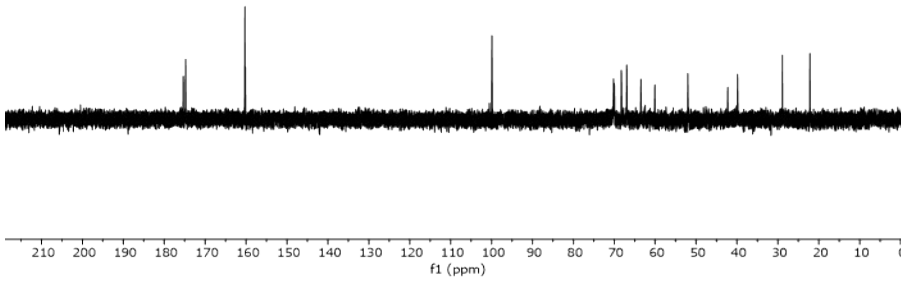
210 200 190 180 170 160 150 140 130 120 110 100 90 80 70 60 50 40 30 20 10
f1 (ppm)

References

(1) El-Boubbou, K.; Gruden, C.; Huang, X. Magnetic Glyco-Nanoparticles: a Unique Tool for Rapid Pathogen Detection, Decontamination, and Strain Differentiation *J. Am. Chem. Soc.* **2007,** *129*, 13392-13393.

(2) Hayes, W. O., H. M.; Osborne, S. D.; Rastall, R. A.; Romagnoli, B. One-Pot Synthesis of Multivalent Arrays of Mannose Mono- and Disaccharides *Tetrahedron* **2003,** *59*, 7983-7996.

(3) Davis, B. G.; Wood, S. D.; Maughan, M. A. Towards an Unprotected Self-Activating Glycosyl Donor System: Bromobutyl Glycosides *Can. J. Chem.* **2002,** *80*, 555-558.

(4) Ladmiral, V. M., G.; Clarkson, G. J.; Cauet, S.; Irwin, J. L.; Haddleton, D. M. Synthesis of Neoglycopolymers by a Combination of “Click Chemistry” and Living Radical Polymerization *J. Am. Chem. Soc.* **2006,** *128*, 4823-4830.

(5) Joosten, J. A.; Loimaranta, V.; Appeldoorn, C. C.; Haataja, S.; El Maate, F. A.; Liskamp, R. M.; Finne, J.; Pieters, R. J. Inhibition of Streptococcus suis Adhesion by Dendritic Galabiose Compounds at Low Nanomolar Concentration *J. Med. Chem.* **2004,** *47*, 6499-6508.

(6) El-Boubbou, K.; Zhu, D. C.; Vasileiou, C.; Borhan, B.; Prosperi, D.; Li, W.; Huang, X. Magnetic Glyco-Nanoparticles: a Tool to Detect, Differentiate, and Unlock the Glyco-codes of Cancer via Magnetic Resonance Imaging *J. Am. Chem. Soc.* **2010,** *132*, 4490-4499.

(7) Tasnima, N. Y., H.; Yan, X.; Li, W.; Xiao, A.; Chen, X. Facile Chemoenzymatic Synthesis of Lewis a (Lea) Antigen in Gram-Scale and Sialyl Lewis a (sLea) Antigens Containing Diverse Sialic Acid Forms *Carbohydr. Res.* **2019,** *472*, 115-121.